

Mixing it up: Inflation at risk*

Maximilian Schröder¹

¹BI Norwegian Business School and Norges Bank

November 19, 2023

Abstract

Measuring and monitoring macroeconomic uncertainty has become a key concern of contemporary monetary policy and an active field of academic research. In this paper, a joint approach is proposed that allows to construct risk measures that capture the unknown and non-standard distribution of inflation and at the same time are consistent with central bank preferences. In addition, two algorithms are proposed that enable to monitor how economic predictors affect the risk outlook and how they shift probability mass across the forecast distribution. Both are widely applicable, enhance the interpretability of a broad class of models, and are suitable for real-time applications. In the empirical exercises, the model yields superior point and density forecasts of U.S. CPI inflation. In addition, during the recent high-inflation period, inflation risk predominantly increased due to a recovery of the U.S. business cycle and rising commodity prices and was in part balanced by monetary policy and credit spreads.

Keywords: inflation, inflation risk, Bayesian methods, density regression, MCMC

JEL Classification: C11, C22, C51, C55, E31

*I would like to thank Sylvia Kaufmann, Sylvia Frühwirth-Schnatter, Hilde Bjørnland, Silvia Miranda-Agrippino, Dimitris Korobilis, Leif A. Thorsrud, Jim Griffin, Fabio Canova, Michele Lenza, Francesco Ravazzolo, Francesco Furlanetto, Domenico Giannone, Giorgio Primiceri, Herman van Dijk, Ørjan Robstad, Lennart Brandt, Frank Schorfheide, and participants at the following conferences for useful comments and discussions: 12th European Seminar on Bayesian Econometrics in Glasgow, 3rd Sailing the Macro Workshop in Siracusa, 3rd Dolomiti Macro Meeting in San Candido, Junior Workshop in Econometrics and Applied Economics in Rome. I would also like to thank seminar participants at the following institutions: BI Norwegian Business School; Norges Bank. The views expressed are those of the authors and do not necessarily reflect those of Norges Bank or any of the affiliated institutions. This paper is part of the research activities at the Centre for Applied Macroeconomics and Commodity Prices (CAMP) at the BI Norwegian Business School.

1 Introduction & Motivation

Contemporary monetary policy has adapted crucial elements of risk management (Greenspan, 2004; Kilian and Manganelli, 2008). Reliable risk measures that accurately capture the uncertainty surrounding economic projections have hence become a necessity in the policy making process. For this purpose, the economic risk management literature formulates two formal requirements that guide the construction of risk measures: (1) The risk measure needs to reflect the underlying distribution of the outcome variable and (2) it needs to be directly linked to the central bank's preferences (Kilian and Manganelli, 2007, 2008; Machina and Rothschild, 1987). The simple example in Kilian and Manganelli (2007) illustrates this. Suppose a central bank has a choice between a scenario (a) 2.0001% inflation with certainty or a scenario (b) 10% inflation with 20% probability and below 2% inflation with 80% probability. In practice, policy makers likely prefer scenario (a) over (b). This implies that the central bank is not indifferent to the size of the target deviation, but instead has preferences over risks. A purely statistical measure of risk; however, would indicate risk to be lower in scenario (b) and provide an inconsistent risk outlook.

In practice, computing risk measures according to these criteria is faced with intricate modelling challenges. The economic uncertainty literature finds ample evidence that economic aggregates have non-standard distributions that are skewed, fat-tailed, and potentially multimodal. For inflation, distributional asymmetries are observed by Banerjee et al. (2020), Korobilis et al. (2021), Korobilis (2017), Lopez-Salido and Loria (2022), and Tagliabruni (2020). Similarly, Adrian et al. (2019) find that the forecast distribution of GDP is negatively skewed especially during recessions. So far; however, the risk management literature has focused the analysis on simple time series models with stochastic-volatility and Gaussian error distributions. This suggests that the derived risk measures do not fully reflect the forecast distribution of the economic aggregate as mandated by criterion (1). In practice, tail risks which are particularly important for policy considerations might hence be especially misrepresented.

In contrast, the economic uncertainty literature constructs risk measures based on predicted quantiles (Koenker and Bassett, 1978) of the economic outcome variable, ignoring central bank preferences and disregarding criterion (2). Even though QRs do not require parametric assumptions on the outcome distribution, they do not yield an estimate of the full forecast distribution, violating criterion (1). As a remedy, the literature proposes estimating separate QRs for different percentile levels. These are then matched to the percentiles of a parametric distribution (e.g. Lopez-Salido and

Loria, 2022). However; approximation error resulting from the independently estimated QRs (Koenker and Bassett, 1978; Chernozhukov et al., 2010), as well as the assumed parametric shape, might again result in an inaccurate measure of the forecast distribution.

Finally, to explore research questions such as “What predicts inflation risk historically/during the recent high inflation period?” it is necessary to extract drivers of risk. In applied policy work, drivers are also required to construct early-warning indicators. Approaches based on standard time-series regression models as in Kilian and Manganelli (2007); however, only allow to monitor how changes in the predictor variables affect global features of the forecast distribution, such as the conditional mean or the conditional variance. Conversely, QRs only provide insights into how predictors impact specific percentiles and hence local features. To truly model the drivers of risk instead, an approach is required that measures how changes in predictor variables shift probability mass dynamically across the forecast distribution. Such a framework is so far missing in the literature.

As a solution, this paper proposes a joint approach for measuring macroeconomic risk, extracting preference consistent risk measures, and monitoring their drivers, under unknown distributions. To satisfy criterion (1) and acknowledge the findings in the economic uncertainty literature, the modeling strategy builds on a semiparametric density regression approach that accurately captures the non-standard distribution of economic aggregates. To take into account central bank preferences and hence satisfy criterion (2), risk measures are constructed based on probability weighted target deviations following Kilian and Manganelli (2007, 2008). The authors establish equivalence between a risk managing and a utility maximizing central bank lending strong theoretical support to this approach and linking it formally to the macroeconomics and central banking literature. Finally, to extract drivers of risk, this paper motivates two new algorithms that are inspired by the literature on interpretable machine learning and Strumbelj and Kononenko (2010) in particular.

Throughout this paper, the proposed framework is applied to inflation and inflation risk, in line with studies such as Banerjee et al. (2020), Kilian and Manganelli (2007), Korobilis et al. (2021), Korobilis (2017), Lopez-Salido and Loria (2022), and Tagliabracchi (2020), but remains applicable to other key economic aggregates.

The empirical section can be split into five exercises. To validate that the model indeed yields accurate estimates of the predictive U.S. CPI inflation distribution, as a first exercise a pseudo out-of-sample forecasting exercise is conducted. The model yields more accurate point forecasts than competing models and the forecast densities are well

calibrated especially up to one year ahead. The results also suggest that accounting for asymmetries in the predictive inflation distribution is important for short and medium term forecast horizons.

The second exercise computes the risk measures in-sample assuming different central bank preferences. Historically, the highest levels of inflation risk are attained during the 1970s and 1980s as well as during the recent inflation surge. Assuming risk-averse central bank preferences, inflation risk was markedly higher in the mid 1970s and the early 1980s, suggesting that the average size of expected target deviations was significantly higher during the pre-Volcker and Volcker-era than towards the end of the sample. Next, as a comparison, the exercise computes risk measures assuming a constant Gaussian and heteroskedastic Gaussian error distribution. For most periods, the results are rather similar; however, pronounced differences emerge during periods of extreme inflation and deflation risk, such as during the Volcker-era or during recessions, i.e. periods where accurate risk measures are most important. These differences become larger for longer forecast horizons.

The third exercise computes the optimal interest rate that minimizes the central bank's loss function under risk aversion, following the results in Svensson (1997). Even though the implied policy rate is computed abstracting from other central bank targets, it is highly correlated with the federal funds rate and broadly follows the same pattern. Interest rate movements during booms and recessions; however, are generally exaggerated.

The fourth exercise computes the drivers of risk. Generally, the U.S. and global business cycle emerge as drivers of downside risks particularly during recessions and the Covid-19 lockdown. In contrast, commodity prices emerge as drivers of upside risks during the first Gulf war, the energy price shocks of 2007 and 2008, the oil price shocks of 2011 and 2017, and the recent high inflation period. Monetary policy and credit spreads mostly emerge as a counter-cyclical driver of risks, driving upside pressure during recessions and downward pressure during periods of high inflation risk.

The final empirical exercise, decomposes the forecast distributions of the four quarters from 2021Q3 to 2022Q2 into its underlying drivers. During this time, the forecast distribution becomes increasingly centered on high inflation realizations, fat-tailed, and left-skewed. These features are mostly driven by the business cycle and commodity prices, which move probability mass from around target realizations towards extreme realizations, whereas monetary policy mostly shifts mass in the opposite direction.

Methodologically, the paper contributes to several strands of the literature. First, the proposed framework unifies the literature on inflation risk with the literature on

central bank risk management. By allowing for unknown and non-standard error distributions, the proposed framework abandons the restrictive assumption of symmetric Gaussian distributions imposed in the risk management literature (e.g. Kilian and Manganelli, 2007), and hence acknowledges the findings in Banerjee et al. (2020), Korobilis et al. (2021), Korobilis (2017), Lopez-Salido and Loria (2022), and Tagliabruni (2020). This improves the overall fit of density forecasts and accuracy of derived risk measures. Conversely, because the approach yields a full properly defined PDF, this allows the construction of preference consistent risk measures, going beyond QRs that have emerged as the workhorse model in the economic uncertainty literature. The results is a flexible and unified risk assessment framework.

Second, the paper contributes to the growing literature on mixture models in economics. In general, mixture models capture real-world data features such as multimodality, skewness, kurtosis and unobserved heterogeneity well (Frühwirth-Schnatter, 2006) and have been successfully applied in the economics literature by Geweke and Keane (2007) to model earnings data and S&P500 returns and by Villani et al. (2009) to study the S&P500 return volatility and non-linearities in the volatility and persistence of U.S. inflation. The mixture model in this paper differs in that it employs the logistic-stick-breaking prior in Rigon and Durante (2020). Under this model formulation, the mixture model attains a conditionally Gaussian structure and collapses to a sequence of linear regression problems. This allows for the implementation of simple and fast estimation algorithms that are particularly easy to use in practice.

To mitigate overfitting in out-of-sample exercises or applications with many predictors, as is common in economics, the horseshoe prior of Carvalho et al. (2010) is imposed on the regression parameters that govern the mixture weights. This results in an MCMC sampler for in-sample exercises and an approximate VB algorithm that is particularly useful in out-of-sample forecasting and real-time exercises, extending the algorithms in Rigon and Durante (2020).

Finally, this paper proposes two new algorithms that allow to monitor drivers of the preference consistent risk measures and the forecast distribution more generally. The first algorithm allows tracking which variables affect arbitrary parts of the predictive distribution of future economic realizations, while preserving integrability. This makes density forecasts generated with the proposed model unique and particularly interpretable. In addition, this algorithm is universal in that it can generally be applied to interpret forecast densities generated with other semi-parametric and mixture models, further contributing to these strands of the literature. The second algorithm allows to decompose the final risk measure into its underlying drivers in real-time. This tool is

particularly useful in applied work and helps to identify which economic variables pose particular risk factors at a given point in time, taking into account the central bank's preferences. Both algorithms have their theoretical foundation in game theory ([Shapley, 1953](#)) and are inspired by the work of ([Strumbelj and Kononenko, 2010](#)) in explainable machine learning.

The remainder of the paper is organized as follows. The next section introduces the risk measures and the density regression framework. Section 3 and 4 describe the estimation algorithms and data. Section 5 discusses the results of the forecasting exercise, section 6 constructs the risk measures and evaluates them empirically, and section 7 and 8 introduce the framework for extracting drivers of risk and the forecast distribution and provide empirical results. The final section concludes.

2 Theoretical Foundations & Empirical model

2.1 The Risk management problem

Following the definition of [Bernanke \(2003\)](#), a central bank concerned with price stability seeks to evade deflation as well as excessive inflation risks, resulting in a trade-off. To measure and summarize these risks and to adapt policy measures to respond accordingly, a central bank requires reliable risk measures. The risk measurement literature identifies two formal requirements. Adapted to inflation risk, (1) the risk measure needs to reflect the underlying probability distribution of future inflation and (2) it must be directly linked to the central bank's pricing of inflation risks ([Machina and Rothschild, 1987](#)).

Formally, upside risks can be viewed as inflation, denoted by π , overshooting an upper threshold, $\bar{\pi}$, and downside risks as π falling short of a lower bound, $\underline{\pi}$, where $\underline{\pi} \leq \bar{\pi}$. For point targets, such as the FED's inflation target, we have that $\underline{\pi} = \bar{\pi} = \pi^*$. Following [Kilian and Manganelli \(2007, 2008\)](#), a general measure of deflation and excessive inflation risk is now given by probability weighted target deviations

$$DR_\alpha \equiv - \int_{-\infty}^{\underline{\pi}} (\underline{\pi} - \pi)^\alpha dF_\pi(\pi), \text{ with } \alpha \geq 0 \quad (1)$$

$$EIR_\beta \equiv \int_{\bar{\pi}}^{\infty} (\pi - \bar{\pi})^\beta dF_\pi(\pi), \text{ with } \beta \geq 0, \quad (2)$$

where DR_α and EIR_β denote deflation risk and excess inflation risk, respectively, and $F_\pi(\pi)$ denotes the distribution of inflation.

The risk aversion/preference parameters are denoted by α and β . In the case of $\alpha = \beta = 0$, the risk measures collapse to the marginal distribution of inflation. Under this regime, the central bank only values excess inflation in either direction, but does not consider the size of the target deviation. For $\alpha = \beta = 1$, the risk measure collapses to a weighted measure of expected shortfall and for $\alpha = \beta = 2$ the risk measures resemble a weighted measure of the target semi-variance. Both incorporate the size of the target deviation, but $\alpha = \beta = 2$ penalizes larger target deviations more strongly than smaller ones. For a risk averse central bank, this specification provides a useful benchmark specification (Blinder, 1997; Kilian and Manganelli, 2007; Svensson, 1997, 2002).

Besides their flexible yet simple form, these risk measures have another advantage. Under mild conditions Kilian and Manganelli (2008) establish equivalence between a risk-managing central bank and an expected utility maximizing central bank for suitably chosen loss functions. A natural choice of a loss function satisfying these properties is

$$L = w \cdot \mathbb{I}(\underline{\pi} < \pi)(\underline{\pi} - \pi)^\alpha + (1 - w) \cdot \mathbb{I}(\bar{\pi} > \pi)(\bar{\pi} - \pi)^\beta,$$

where w is a weight parameter with $0 \leq w \leq 1$. Taking expectations yields the balance of risk, $BR_{\alpha,\beta}$, or expected loss

$$BR_{\alpha,\beta} \equiv E(L) = -wDR_\alpha + (1 - w)EIR_\beta. \quad (3)$$

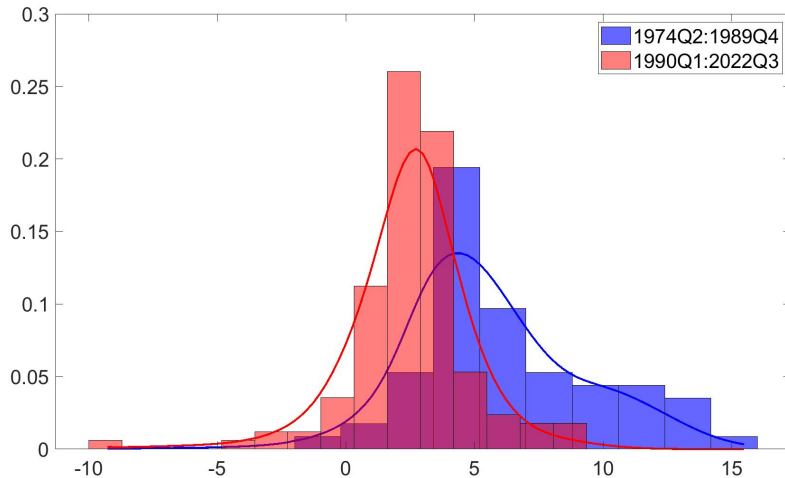
This risk modelling framework is hence fully consistent with standard approaches of modelling the central banks decision problem and remains consistent for a broad range of preference functions. This includes non-integer values for α and β , different combinations of both parameters or policy-regime-specific parameter settings. As an example, towards the end of the Covid-19 pandemic, policy makers were cautious to raise rates too quickly and hence forestall the nascent recovery. In this scenario, the central bank's preferences might have been more accepting of higher inflation rates, suggesting $\beta < \alpha$ or $w < 0.5$. Conversely, during periods when policy rates are constrained by the effective lower bound, a central bank might be particularly concerned about deflationary pressures. This can be accommodated by setting $w > 0.5$.

Purely statistical measures of risk such as the conditional variance, skewness, or extreme quantiles of the inflation distribution, are completely invariant to preferences and changes in preferences. This results in an incomplete measure of risk or implicitly assumes central bank preferences that are unrealistic or inconsistent with the central banking literature at the least.

2.2 Density Regression

A critical ingredient of the risk measures introduced in the previous section is a measure of the full underlying distribution of future inflation. The classical risk management literature focuses on “risk”, i.e. uncertainty bounded by a known probability distribution. The literature on inflation uncertainty; however, provides ample evidence that the distribution of inflation is non-standard (Banerjee et al., 2020; Korobilis et al., 2021; Korobilis, 2017; Lopez-Salido and Loria, 2022; Tagliabracci, 2020).

Figure 1: Annualized Quarterly Inflation



Notes: The histograms display the observed values for annualized quarterly inflation from 1974Q1 to 1889Q4 (blue) and from 1990Q1 to 2022Q3 (red). The corresponding lines show the density estimates over these sub-samples, obtained with the density regression model estimated over the full sample with MCMC.

Figure 1 provides illustrative evidence. The figure shows the histograms of the annualized quarterly inflation rate as well as fitted distributions over the sub-samples from 19974Q1 to 1989Q4 and from 1990Q1 to 2022Q3, respectively. In both samples, the distributions are strongly skewed and fat-tailed. In addition, the distributions vary in their characteristics across the two samples and do not seem directly related to well known parametric families.

In light of this evidence, this paper takes a different approach that accounts for the unknown nature of the distribution of inflation. As a starting point, let the predictive density of inflation for a forecast horizon h be expressed as

$$f(\pi_{t+h}) = \int K(\pi_{t+h}; \boldsymbol{\theta}) p(d\boldsymbol{\theta}),$$

where $K(\pi_{t+h}; \boldsymbol{\theta})$ denotes a parametric kernel and p denotes a probability measure.

Following Ishwaran and James (2001) and imposing a stick-breaking representation on p , gives rise to an infinite mixture model

$$f(\pi_{t+h}) = \int K(\pi_{t+h}; \boldsymbol{\theta}) p(d\boldsymbol{\theta}) = \sum_{c=1}^{\infty} w_c K(\pi_{t+h}; \boldsymbol{\theta}_h),$$

where $w_c = \nu_c \prod_{l=1}^{c-1} (1 - \nu_l)$ and $w_1 = \nu_1$, denote the stick breaking weights, for every $c \geq 1$.¹

As with other forecasting models for inflation, it is desirable to let the individual Kernels as well as the mixture component weights depend on observable predictors (also see Geweke and Keane, 2007; Villani et al., 2009), such as the interest rate, proxies for energy prices, or the state of the business cycle. The relevant methodological generalizations are introduced by De Iorio et al. (2004), Gelfand et al. (2005), and De la Cruz-Mesía et al. (2007) and Dunson and Park (2008), Griffin and Steel (2006), and Gutiérrez et al. (2016), respectively. This leads to mixture representation

$$f_x(\pi_{t+h}) = \int K_{\mathbf{x}}(\pi_{t+h}; \boldsymbol{\theta}) p_x(d\boldsymbol{\theta}) = \sum_{c=1}^{\infty} w_c(\mathbf{x}_t) K_{\mathbf{x}}(\pi_{t+h}; \boldsymbol{\theta}_h), \quad (4)$$

where $w_c(\mathbf{x}_t) = \nu_c(\mathbf{x}_t) \prod_{l=1}^{c-1} (1 - \nu_l(\mathbf{x}_t))$.

Although offering significant flexibility, standard estimation algorithms are accompanied by substantial computational cost. Recently, Rigon and Durante (2020) propose a model variant building on the work of Polson et al. (2013), Ren et al. (2011), Rodrigues and Dunson (2011), and Tutz (1991) that allows for the derivation of computationally simple and efficient estimation algorithms that are at the core of the econometric framework proposed in this paper. The key innovation in Rigon and Durante (2020) is to relate the stick-breaking weights, $\nu_c(\mathbf{x})$, to a function of the covariates, \mathbf{x} , via the logistic link. This results in a Logit stick-breaking prior (LSBP).

The functionality of the approach rests on three main results, which are restated here - applied to inflation modelling - for readers unfamiliar with the subject. The individual steps follow Rigon and Durante (2020). First, the stick-breaking prior admits a continuation-ratio parameterization as in Tutz (1991). Rewriting the model in Equation (4) in its hierarchical representation, yields

¹Any smooth density can be approximated by a Gaussian mixture model to arbitrary degrees of accuracy, given a large enough number of mixture components (Goodfellow et al., 2016).

$$(\pi_{t+1} | \mathbf{G}_t = c, \mathbf{x}_t) \sim K_{\mathbf{x}_t}(\pi_{t+1}; \boldsymbol{\theta}_c), \text{ with } \text{pr}(G_t = c | \mathbf{x}_t) = w_c(\mathbf{x}_t) = \nu_c(\mathbf{x}_t) \prod_{l=1}^{c-1} (1 - \nu_l(\mathbf{x}_t)), \quad (5)$$

for each $t = 1, \dots, T$, with $\boldsymbol{\theta}_c$ distributed independently for each mixture component, c . G_t denotes a categorical variable that stores the mixture component allocation at time t and has probability mass function $f(G_t | \mathbf{x}_t) = \prod_{c=1}^{\infty} w_c(\mathbf{x}_t)^{\mathbb{I}(G_t=c)}$, where $\mathbb{I}(\cdot)$ denotes the indicator function. This allows to rewrite the stick-breaking weights, $\nu_c(\mathbf{x}_t)$, as a function of the mixture probabilities $w_c(\mathbf{x}_t)$

$$\nu_c(\mathbf{x}_t) = \frac{w_c(\mathbf{x}_t)}{1 - \sum_{l=1}^{c-1} w_h(\mathbf{x}_t)} = \frac{\text{pr}(G_t = c | \mathbf{x}_t)}{\text{pr}(G_t > c - 1 | \mathbf{x}_t)}, \text{ with } f \in \mathbb{N}. \quad (6)$$

Now the stick-breaking weights, $\nu_c(\mathbf{x}_t)$, can be interpreted as the probability of being allocated to mixture component c , conditional on not being allocated to the previous $1, \dots, c-1$ mixture components ([Rigon and Durante, 2020](#)). The infinite mixture problem can hence be broken up into $c-1$ sequential binary choice problems. In the first step, a given observation is either allocated to the first component, $c = 1$, with probability $\nu_1(\mathbf{x}_t)$ or any of the subsequent components, $c : h > 1$, with probability, $1 - \nu_1(\mathbf{x}_t)$. This procedure is then repeated for subsequent components and terminates once $G_t = 1$.

Second, one can now rewrite the continuation-ratio representation and introduce an assignment indicator $\zeta_{tc} = \mathbb{I}(G_t = c)$ given by

$$\zeta_{tc} = z_{tc} \prod_{l=1}^{c-1} (1 - z_{tl}) \quad (7)$$

for each $t = 1, \dots, T$. $z_{tc} \sim \text{Bern}(\nu_1(\mathbf{x}_t))$ is a Bernoulli random variable that encodes the decision of allocating a given observation to component c or any of the subsequent ones. [Rigon and Durante \(2020\)](#) introduce the logistic link into this sequential Bernoulli choice problem. To see this, define $\eta_c(\mathbf{x}_t) = \text{logit}(\nu_c(\mathbf{x}_t)) = \log(\nu_c(\mathbf{x}_t)/(1 - \nu_c(\mathbf{x}_t)))$, and combine the result with Equation (5). This yields the logit stick-breaking prior on $w_c(\mathbf{x}_t)$

$$w_c(\mathbf{x}_t) = \frac{\exp\{\eta_c(\mathbf{x}_t)\}}{1 + \exp\{\eta_c(\mathbf{x}_t)\}} \prod_{l=1}^{c-1} \left[\frac{1}{1 + \exp\{\eta_c(\mathbf{x}_t)\}} \right], \quad (8)$$

where $\eta_c(\mathbf{x}_t)$ is the log-odds of the probability of observation t being allocated to component c conditional on not having been allocated to any of the previous components. This allows to estimate the parameters governing the stick-breaking

weights by a series of logistic regressions.

The stick-breaking formulation has an additional advantage. In practice, the sequential structure induces shrinkage. Redundant components that are not required to characterize the data are deleted, keeping the model parsimonious and computationally tractable. Specifically, because the above procedure terminates whenever $G_t = 1$, later components might never be reached and hence receive a zero probability.

Finally, this formulation allows to leverage the results in Polson et al. (2013) that offer computational advantages in case of Bayesian logistic regression through Pólya-Gamma augmentation. Essentially, conditional on a Pólya-Gamma distributed variable $\omega_{t,h} \sim PG(1, \mathbf{x}'_t \boldsymbol{\phi}_c)$, the logistic regression collapses to a linear regression of the transformed assignment decision indicators $(z_{tc} - 0.5)/\omega_{t,h}$ onto the predictors \mathbf{x}_t (Polson et al., 2013; Rigon and Durante, 2020). Compared to e.g. Metropolis–Hastings (MH) samplers, this approach is computationally fast, automatic, and requires no parameter tuning. These features make it especially suitable for large hierarchical models.

2.3 Likelihood, Priors and Posterior

With the general framework in place, what remains is the specification of the likelihood function and priors. For the individual mixture components in Equation 4,

$$K_{\mathbf{x}}(\pi_{t+h}; \boldsymbol{\theta}) = \sqrt{\tau_c} \phi(\sqrt{\tau_c}(\pi_{t+h} - \mathbf{x}_t \boldsymbol{\beta}_c)), \quad (9)$$

is assumed, where $\mathbf{x}_t = [x_{t,1}, \dots, x_{t,n}]$ collects the constant, lags of inflation, and additional explanatory variables for $t = 1, \dots, T$. ϕ denotes the Gaussian kernel, $\tau_c = \sigma_c^{-2}$ is the corresponding precision parameter, and $\boldsymbol{\beta}_c$ denotes the kernel specific regression coefficients. Correspondingly, Equation 4 is now given by

$$f_x(\pi_{t+h}) = \sum_{c=1}^{\infty} w_c(\mathbf{x}) \sqrt{\tau_c} \phi(\sqrt{\tau_c}(\pi_{t+h} - \mathbf{x}_t \boldsymbol{\beta}_c)). \quad (10)$$

As a result, every mixture component is characterized by the same predictive relationship; however, the individual regression parameters are free to differ. The cluster allocation of each observation is governed by the categorical, G_t , which depends on the mixture probabilities, w_c , and hence the log-odds. Throughout the paper, it is assumed that $\eta_c(\mathbf{x}_t)$ depend linearly on \mathbf{x}_t . This yields $\eta_c(\mathbf{x}_t) = \mathbf{x}'_t \boldsymbol{\psi}_c$.

In practice, the framework can accommodate different sets of predictors for the kernels and the log-odds. In forecasting applications for example it might be useful to let the mixture probabilities depend on a large set of covariates that broadly reflect the

state of the economy, while keeping a parsimonious structure for the individual mixture components. However; like linear regression, logistic regression also suffers from the curse of dimensionality, if the number of variables grows large. Similarly, it is beneficial to penalize the likelihood in out-of-sample forecasting applications to enforce parsimony.

To address these issues, the horseshoe prior proposed in [Carvalho et al. \(2010\)](#) is placed on the parameters ψ_c , where

$$\psi_c | \xi_c, \bar{\tau}_c \sim \prod_{j=1}^k N(0, \xi_c \bar{\tau}_{j,c}) \quad (11)$$

$$\xi_c \sim C^+(0, 1) \quad (12)$$

$$\bar{\tau}_{j,c} \sim C^+(0, 1), \quad (13)$$

and C^+ denotes the half-Cauchy distribution. Under the horseshoe prior, the posterior remains almost unrestricted in small parameter spaces; however, as the parameter space grows large relative to the number of observations, increasing amounts of shrinkage are imposed. In addition, it is automatic and parameter tuning free and has hence become the default choice for many researchers ([Korobilis and Shimizu, 2022](#)).

Due to the conditionally normal form of the individual logistic regressions, the prior can be imposed without adjustments and sampling proceeds as in the standard regression case. The application of the horseshoe prior in the density regression context is novel. However; [Bhattacharyya et al. \(2022\)](#) and [Wei and Ghosal \(2020\)](#) find that the favourable properties of the horseshoe prior carry over to Bayesian logistic regression. Because independent horseshoe priors are assigned to each mixture component, in application this facilitates the formation of independent clusters or inflation regimes.

To complete the description of the priors, $\tau_c \sim IG(a_\tau, b_\tau)$, $\beta_c \sim N(0, 1)$, and the LSBP in Equation (8) are imposed on the kernel specific precision parameter τ_c , the kernel regression coefficients and the mixing probabilities $w_c(z_t)$, respectively. Finally, in application the algorithm operates on a truncated version of the probability measure p_x that serves as an approximation to the infinite mixture model. For a truncation point C , only the first $C - 1$ components are modeled and $\nu_C = 1$ for all $\mathbf{x} \in \mathcal{X}$, such that $\sum_{c=1}^C w_c(\mathbf{x}) = 1$. [Rigon and Durante \(2020\)](#) show that this approximation is accurate, as long as the truncation point is set sufficiently large. The joint posterior of the model is hence given by

$$p(\Theta|y) = \prod_{t=1}^T \left[\prod_{c=1}^C \sqrt{\tau_c} \phi(\sqrt{\tau_c}(\bar{\pi}_{t+h} - \mathbf{x}_t \boldsymbol{\beta}_c))^{\mathbb{I}(G_t=c)} \prod_{c=1}^{C-1} \nu_c(\mathbf{z}_t)^{\mathbb{I}(G_t=c)} (1 - \nu_l(\mathbf{z}_t))^{\mathbb{I}(G_t>c)} \right] \\ \cdot \prod_{c=1}^{C-1} p(\boldsymbol{\psi}_c|\xi_c, \bar{\tau}_c) p(\xi_c) \prod_{j=1}^k p(\bar{\tau}_{j,c}) \cdot \prod_{c=1}^C p(\boldsymbol{\beta}_c) p(\tau_c),$$

where $\nu_c(\mathbf{x}_t) = \exp\{\mathbf{x}'_t \boldsymbol{\psi}_c\} / [1 + \exp\{\mathbf{x}'_t \boldsymbol{\psi}_c\}]$ and Θ collects all model parameters. In all empirical exercises, $C = 5$ is assumed. For readers interested in an automatic procedure, appendix C.2 details a simple algorithm for estimating the number of mixture components.

3 Estimation Algorithm

To estimate the model, two complementary estimation algorithms are proposed, a MCMC sampler and a Variational Bayes algorithm, extending the algorithms in Rigon and Durante (2020). In practice, both, MCMC and VB, provide approximations to the posterior distribution. Whereas MCMC provides approximations through sampling, VB solves an optimization problem. Both algorithms are iterative; however, VB requires sufficiently less iterations and is hence computationally faster, contributing to its popularity in the machine learning literature. As a caveat, compared to MCMC which guarantees accurate samples from the posterior, VB generally provides an approximate solution. Overall, VB is thus particularly useful for big data applications, large scale forecasting exercises or real-time monitoring tasks, which are frequent in applied policy work.²

In the remainder of the paper, the MCMC algorithm is used for generating results on the full sample, where computational demand is less of a concern and VB is used in the forecasting and out-of-sample exercises. To provide evidence that the results are generally comparable, Figure 7 (8) in the appendix shows the estimated inflation densities (risk measures) estimated with both algorithms over the full sample. In both cases, the algorithms yield very similar results. This suggests that only little accuracy is sacrificed by using VB in the context of the application in this paper.

For the sake of brevity and because both algorithms generally follow the same steps, the below outlines the steps of the MCMC sampler:

1. Sample the mixture indicator G_t from a categorical distribution with probability

²For a general introduction to VB see Blei et al. (2017).

$pr(G_t = c)$ and assign each observation to the corresponding mixture component. This step is implemented as in [Rigon and Durante \(2020\)](#).

2. Sample the parameters of the individual logistic regressions that govern the mixture component allocation, ψ_c . This step exploits the Pólya-gamma augmentation scheme for Bayesian logistic regression of [Polson et al. \(2013\)](#) as well as the continuation-ratio formulation introduced above. In particular, for each mixture component, $c = 1, \dots, C - 1$, subset the observations for which $G_t > c - 1$ into two groups and define indicator variable $\bar{z}_{t,c}$, such that $\bar{c}_{t,c} = 1$, if $G_t = c$ and $\bar{z}_{t,c} = 0$, if $G_t > c$. Conditional on a draw of the Pólya-gamma distributed variable $\omega_{t,c} \sim PG(1, \mathbf{z}'_t \boldsymbol{\psi}_c)$ the likelihood contribution of observation t is proportional to a Gaussian kernel for $(\bar{z}_{tc} - 0.5)/\omega_{t,c}$. The mixture parameters, ψ_c , can now be updated exploiting standard results for Bayesian linear regression.
3. Sample the parameters of the horseshoe prior based on the hierarchical parametrization of [Makalic and Schmidt \(2016\)](#). This parametrization has the advantage that it leads to conjugate posterior distributions and hence facilitates the implementation of fast and simple samplers.
4. Sample the kernel specific regression and precision parameters, $\boldsymbol{\beta}_c$ and τ_c , exploiting the results for standard Bayesian linear regression.

Overall, the algorithm collapses to a sequence of Bayesian linear regressions and has a simple and user-friendly structure. The full algorithms, which are extensions of the algorithms in [\(Rigon and Durante, 2020\)](#) and additional derivations are provided in appendix A. Throughout the paper, MCMC results are based on 1,000,000 draws, after discarding the initial 100,000 draws of the chain. Out of the remaining draws, only every 100th is retained, as consecutive draws might be strongly correlated.

4 Data

Throughout this paper, a baseline dataset of key U.S. and global variables is used that spans the period from 1973Q2 to 2022Q3. An overview is provided in table 1. In all exercises, the target variable is the annualized U.S. quarterly CPI inflation rate.

Overall, the selection of variables is in line with the Phillips curve and inflation forecasting literature such as [Koop and Korobilis \(2012\)](#), [Korobilis \(2017\)](#), [Lopez-Salido and Loria \(2022\)](#), and [Stock and Watson \(1999, 2010\)](#), adding global indicators that are

discussed as important inflation drivers during the Covid-19 pandemic and recent high inflation period. Because later exercises are aimed at illustrating drivers of risk and the forecast distribution, indicators of the domestic U.S. economy are included as a factor instead of individual series to simplify interpretation. In particular, this activity factor is extracted from the panel of variables in the FRED-QD³ database developed by McCracken and Ng (2020) with partial least squares. To retain as much information on future inflation as possible, the factor is extracted for one-step ahead inflation. Prior to factor extraction, broad aggregates are excluded following Stock and Watson (2012) and the data is transformed to stationary following the authors' recommendations.

Table 1: Data Overview

MACROECONOMIC INDICATORS	SOURCE	MNEMONICS	TCODE ¹
Consumer price index for all urban consumers	FRED	CPI	4
U.S. business cycle indicator	FRED-QD ²	BC _d	1
Excess Bond Premium	Gilchrist and Zakrajšek (2012) ³	EBP	1
Federal Funds Rate	FRED	FFR	1
OECD+6 industrial production	Baumeister and Hamilton (2019) ⁴	BC _g	4
Energy price index	“Pink Sheet”, The World Bank ⁵	Energy	4
Food price index	“Pink Sheet”, The World Bank ⁵	Food	4
Metal price index	“Pink Sheet”, The World Bank ⁵	Metals	4

¹ Tcode identifies the time series transformation: level (1), log-differences (4).

² The data is taken form the FRED-QD database. The indicator is based on own computations.

³ <https://sites.google.com/site/cjsbaumeister/datasets?authuser=0>.

⁴ <https://www.worldbank.org/en/research/commodity-markets>.

⁵ https://www.federalreserve.gov/econres/notes/feds-notes/ebp_csv.csv.

In line with the economic uncertainty literature (Banerjee et al., 2020; Korobilis et al., 2021; Lopez-Salido and Loria, 2022; Tagliabruni, 2020) the excess bond premium (EBP), constructed by Gilchrist and Zakrajšek (2012), is included as a measure of financial conditions. Gilchrist and Zakrajšek (2012) find that the EBP is particularly informative about future economic activity, making the EBP a forward-looking indicator that captures macro-financial linkages. At the same time, compared to broad indicators of financial conditions such as the NFCI, the EPB is constructed entirely from financial market data and hence less likely to capture information already contained in the macroeconomic variables (Reichlin et al., 2020).

The federal funds rate (FFR) completes the domestic block. In the forecasting exercise the FFR is included without further transformations. In exercises highlighting

³The database spans a large set of economic indicators that cover 14 broad groups - NIPA; industrial production; employment and unemployment; housing; inventories, orders, and sales; prices; earnings and productivity; interest rates; money and credit; household balance sheets; exchange rates; others (uncertainty and expectations); stock markets, non-household balance sheets; - and has found wide applications in economic research.

the drivers of risk; however, the FFR is replaced by a policy proxy to consider the role of monetary policy. In particular, because interest rates are influenced by many factors beyond central bank decisions, this often leads to price or output puzzles in applied research and inaccurate measures of the contribution of monetary policy to inflation risks in later exercises. In this paper, the policy proxy is constructed from high-frequency information by re-running the Proxy-SVAR in [Miranda-Agrippino \(2016\)](#) on an updated sample. The FFR is then replaced with the implied structural monetary policy shock.

Besides the domestic economy, inflation is also largely determined by global factors ([Forbes, 2019](#)). In particular, during the Covid-19 pandemic, the recovery, and the recent high inflation period, global business cycle dynamics and commodity prices have been discussed as drivers of inflation risks (see e.g. [Blanchard and Bernanke, 2023](#)). To proxy global business cycle dynamics, the global industrial production indicator constructed by [Baumeister and Hamilton \(2019\)](#) is included. The index covers the OECD as well as six additional major economies adding up to roughly 75% of the IMF World Economic Outlook estimate of global GDP ([Baumeister and Hamilton, 2019](#)). Commodity prices are proxied by the indices for energy, food, and metal prices from the World Bank’s “Pink Sheet” dataset.

Finally note that all predictors are standardized before estimation. Besides these transformations, the data is not manipulated in any way and in particular not adjusted for the outliers observed during the pandemic.

5 Forecasting Exercise

The density regression framework is motivated by two considerations. First, compared to QRs or standard time series regression models, the mixture formulation allows to back out the drivers of risk in later sections. Second, the flexible form promises to capture the non-standard distribution of inflation more accurately than models that assume symmetric error distributions. To evaluate whether the model actually fits the inflation density better, this section presents a pseudo out-of-sample forecasting exercise and evaluates density as well as point forecasts.

As a set of benchmark models a simple AR-X, a SV-AR-X, a TVP-AR-X, a TVPSV-AR-X, an AR-X with t-distributed residuals (T-AR), and a QR model are included. These models hence capture a wide set of univariate model classes frequently used in economic forecasting exercises. All models and the density regression model include 4 lags of the

annualized quarterly inflation rate and the whole set of predictor variables introduced above. The information set is hence the same across models.

All models are estimated with VB.⁴ In particular, the estimation algorithms for the TVP and SV-AR models are similar to [Koop and Korobilis \(2023\)](#) and the AR with t-distributed errors is estimated with the algorithm in [Christmas and Everson \(2011\)](#). Estimation starts with 50% of the total sample. Each vintage direct forecasts for 1 to 12 quarters ahead are computed. Then the sample is extended with one more observation at the end of the sample, the models are re-estimated, and a new set of forecasts is generated.

Starting with the point forecasts, the RMSEs relative to the AR models for the forecast horizons $h = 1, 2, 3, 4, 8, 12$ are given in table 4. The absolute RMSE and results for all forecast horizons are provided in the appendix. In addition, statistical significance of the Diebold-Mariano test is vis-à-vis the AR model is indicated by the asterisks. A few results stand out. First, only the DR, SV-AR, and T-AR model perform consistently better than the AR model. In case of the DR and SV-AR, the performance improvements are statistically significant for most horizons. For forecast horizons less than one year, the DR model is the best performing model. For longer horizons, the DR and the SV-AR perform on par. On the one hand this indicates that the DR model yields accurate point forecasts, improving upon competitive benchmark models. On the other hand, the results suggest that accounting for asymmetries in the forecast distribution is important for short horizons, but matters less at longer horizons in terms of point forecast performance.

Table 2: Relative RMSE vis-à-vis AR

h	DR	SV-AR	TVP-AR	TVPSV-AR	T-AR
1	0.875***	0.946*	1.294	1.203***	0.987
2	0.824	0.883	1.917*	1.094	0.958
3	0.853*	0.887**	2.201*	0.951	0.952
4	0.913	0.904*	2.801**	0.932	0.958
8	0.844***	0.830***	1.511**	0.977	0.890***
12	0.871**	0.848***	1.692	1.039	0.829***

The table contains the RMSE relative to the AR model. Statistical significance of the Diebold-Mariano test is indicated by the *, where {***} = 1%, {**} = 5%, {*} = 10%.

To evaluate the accuracy of the density forecasts, probability integral transforms (PITs) are constructed. In principle, PITs, are computed as the probability of observing

⁴The entire exercise runs within a few hours on a laptop with Intel Core i5-8265U CPU with 1.6GHz without parallelization.

the realized value given the model's predictive density, i.e. $\text{pit}_{t+h|t} = \int_{-\infty}^{y_{t+h}} f_x(\pi)_{t+h|t} d\pi$. For a correctly specified forecast density, the distribution of the PITs is independent and identically uniform. To formally test whether the PITS fulfill these properties, this paper follows [Rossi and Sekhposyan \(2014\)](#). All tests are implemented using their algorithms. Table 5 presents the results.⁵

Table 3: p-values for tests on PITs

	Uniformity			Identical		Independent		Uniform			Identical		Independent	
	KS	AD	DH	1 st	2 nd	1 st	2 nd	KS	AD	DH	1 st	2 nd	1 st	2 nd
	<i>H</i> = 1													
DR	0.871	0.735	0.214	0.979	0.740	1.000	0.597	0.489	0.364	0.158	0.180	0.966	0.240	0.112
AR	0.007	0.002	0.000	0.322	0.000	0.607	0.097	0.015	0.004	0.000	0.001	0.000	0.884	0.532
SV-AR	0.309	0.053	0.081	0.649	0.878	1.000	1.000	0.345	0.002	0.015	0.001	0.027	1.000	1.000
TVP-AR	0.000	0.000	0.000	0.589	0.005	0.865	0.427	0.000	0.000	0.000	0.200	0.700	0.825	0.814
TVPSV-AR	0.000	0.000	0.000	0.010	0.955	0.000	0.000	0.000	0.000	0.000	0.000	0.001	0.000	0.000
T-AR	0.000	0.000	0.000	0.428	0.019	1.000	0.740	0.000	0.000	0.000	0.001	0.000	0.843	0.450
QR	0.025	0.014	0.000	0.585	0.310	0.657	0.208	0.008	0.011	0.011	0.000	0.036	0.364	0.065
<i>H</i> = 3														
DR	0.280	0.365	0.475	0.037	0.835	0.135	0.100	0.326	0.400	0.715	0.224	0.376	0.769	0.563
AR	0.003	0.002	0.000	0.001	0.002	0.487	0.297	0.053	0.012	0.000	0.001	0.006	1.000	0.754
SV-AR	0.532	0.003	0.171	0.005	0.000	0.891	0.318	0.382	0.000	0.105	0.005	0.002	1.000	0.748
TVP-AR	0.000	0.000	0.000	0.003	0.003	1.000	1.000	0.000	0.000	0.000	0.005	0.044	0.274	0.150
TVPSV-AR	0.000	0.000	0.015	0.000	0.835	0.000	0.000	0.000	0.000	0.056	0.000	0.931	0.000	0.000
T-AR	0.000	0.000	0.000	0.001	0.002	0.173	0.038	0.000	0.000	0.000	0.004	0.009	0.429	0.133
QR	0.001	0.005	0.004	0.000	0.046	0.731	0.289	0.000	0.002	0.000	0.053	0.234	0.550	0.137
<i>H</i> = 8														
DR	0.173	0.054	0.892	0.045	0.612	0.670	0.801	0.521	0.407	0.288	0.000	0.000	0.102	0.043
AR	0.000	0.000	0.015	0.003	0.000	0.201	0.428	0.000	0.000	0.001	0.000	0.000	0.000	0.000
SV-AR	0.117	0.000	0.970	0.001	0.000	0.431	0.085	0.099	0.000	0.263	0.002	0.000	0.000	0.000
TVP-AR	0.000	0.000	0.000	0.341	0.566	1.000	1.000	0.000	0.000	0.000	0.004	0.077	0.049	0.061
TVPSV-AR	0.000	0.000	0.000	0.000	0.500	0.000	0.000	0.000	0.000	0.000	0.000	0.227	0.000	0.000
T-AR	0.000	0.000	0.000	0.008	0.017	0.430	0.799	0.000	0.000	0.000	0.000	0.000	0.162	0.058
QR	0.000	0.001	0.001	0.003	0.001	0.395	0.026	0.000	0.000	0.001	0.000	0.000	0.014	0.016
<i>H</i> = 12														

The table contains the p-values for several test statistics: KS=Kolmogorov-Smirnov, AD=Anderson-Darling, DH=Doornik-Hansen, Andrews, Ljung-Box. For the Andrews and Ljung-Box test, 1st and 2nd denote the results for the first and second moment, respectively. *H* indicates the forecast horizon. Bold values mark p-values greater than 5%.

To test for uniformity, the Kolmogorov-Smirnov (KS), Anderson-Darling (AD) ([Anderson and Darling, 1952, 1954](#)), and Doornik-Hansen (DH) ([Doornik and Hansen, 2008](#)) test statistics are computed. Compared to the KS, the AD test puts more weight on the tails of the distribution and is more powerful especially in smaller samples. The main difference to the DH test is that it tests for the absence of skewness and kurtosis in the inverse normal transformation of the PITs, whereas KS and AD test for uniformity directly.

⁵Results for the test in [Berkowitz \(2001\)](#) are omitted, because they remained inconclusive.

Over all forecast horizons, the KS test does not reject uniformity for the density regression and SV-AR model. For all other models uniformity can be rejected. For the DH and AD test, uniformity is also rejected for the SV-AR model at horizons $h = 2$ and $h = 2, 3, 4, 8, 12$, respectively. Overall, the density regression model proposed in this paper is the only model for which uniformity is not rejected at any forecast horizon under all three tests.

The next test assesses whether the PITs have an identical distribution. This property implies that the moments of the PITs must remain stable over time. Following [Rossi and Sekhposyan \(2014\)](#), the test is implemented by computing the test for structural breaks in [Andrews \(1993\)](#) for the mean and the variance. For the SV-AR, stability cannot be rejected at $h = 1$, but is rejected for all other horizons. For the QR model, stability cannot be rejected at $h = 1$ and $h = 4$, and for the TVP-AR at $h = 2$ and $h = 8$. Importantly, for the density regression model, stability cannot be rejected at $h = 1$, $h = 2$, and $h = 4$ and is just rejected at $h = 3$.

The final test is for independence of the PITs. Following [Rossi and Sekhposyan \(2014\)](#) it is implemented with the Ljung-Box test for the first and second moment. For horizons $h = 1, 2, 4$ the TVPSV-AR is the only model for which independence can be rejected. At $h = 3$ ($h = 4$) independence is also rejected for the T-AR (QR) model. At $h = 12$ the T-AR model is the only model for which independence cannot be rejected. For the density regression model, independence is only rejected at $h = 12$.

Overall, the density regression model produces correctly calibrated density forecasts especially up until the one year ahead horizon, supporting the modeling approach.

6 Risk Measures

6.1 Computing Risk measures

One great advantage of the framework proposed in this paper is its tractable form. Because the predictive density is constructed from a mixture of Gaussian distributions, the exact PDF and CDF of the predictive inflation distribution are readily available from the model. Let Θ^m denote a set of posterior draws and π denote a point of interest. At time t and for draw m the full predictive PDF at π is then given by

$$f_x(\pi)_{t+h|t} = \sum_{c=1}^C \left[\nu_c(\mathbf{x}_t) \prod_{l=1}^{c-1} \{1 - \nu_l(\mathbf{x}_t)\} \right] \cdot \sqrt{\tau_c^m} \phi(\sqrt{\tau_c}(\pi - \mathbf{x}_t \beta_c^m)). \quad (14)$$

Repeating the computation for a set of π values that span the support of $f_x(\pi_{t+h})$ then

yields the entire distribution function at one MCMC draw at time t for forecast horizon $t + h$. Averaging across draws yields the final PDF estimate and credible intervals can be constructed by computing quantiles instead. Finally, the unconditional inflation distribution can be obtained by also averaging across time. For VB, the density can be computed by either plugging in the final VB estimates or by generating samples from the posterior conditional on the estimated parameters. Computations for the CDF follow analogously.

Given central bank preferences, the final risk measures are now given by

$$DR_{\alpha,t+h|t} \equiv - \int_{-\infty}^{\underline{\pi}} (\underline{\pi} - \pi)^\alpha f_x(\pi)_{t+h|t} d\pi, \text{ with } \alpha \geq 0, \quad (15)$$

$$EIR_{\beta,t+h|t} \equiv \int_{\bar{\pi}}^{\infty} (\pi - \bar{\pi})^\beta f_\pi(\pi)_{t+h|t} d\pi, \text{ with } \beta \geq 0. \quad (16)$$

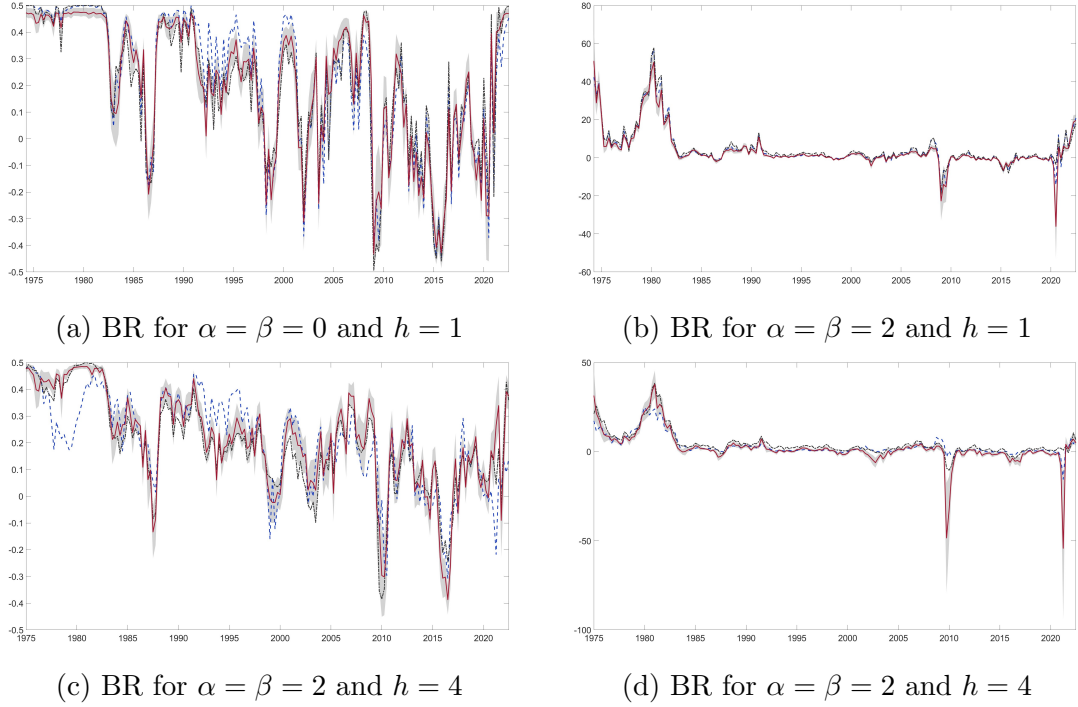
Conditional on the density regression model, they fully account for the non-standard distribution of future inflation. To evaluate the integrals in Equations 15 and 16, Gaussian quadrature methods are used throughout the paper. This results in a fast and simple numerical procedure.

6.2 In-Sample Risk Measures

As a first exercise, this section considers central bank preferences that weight positive and negative target deviations equally. Further, to match the FED’s policy objective of 2% annual inflation, the bounds and weights are set to $\underline{\pi} = \bar{\pi} = 2$ and $w = 0.5$. Figure 2 displays the estimated balance of risk for one quarter ahead inflation in the first row and four quarter ahead inflation in the second row. The shaded area indicates 86% credible intervals. As a benchmark, corresponding estimates obtained from a univariate forecasting model with stochastic volatility and constant volatility, respectively, are indicated by the dashed blue and dot-dashed black line. All models are estimated with MCMC over the full sample of available data. For all risk measures, positive (negative) values indicate excess inflation (deflation) risk.

The left panel shows the results for $\alpha = \beta = 0$. In this case, the risk measure is purely statistical and corresponds to a central bank that only considers the probability of inflation overshooting the target, but not the size of the target deviation. Under this parameter setting, inflation risk was exclusively on the upside until the early 80s for the first forecast horizon, $h = 1$. It then gradually decreased, with an interruption in 1984,

Figure 2: The Balance of Risk



Notes: The solid red line indicates the MCMC estimate over the full sample obtained with the density regression model. The shaded area is the corresponding 86% credible interval. The dashed blue (dot-dashed black) line show the corresponding estimates computed with a model with stochastic volatility and constant volatility, respectively.

falling to a temporary low in 1986. Towards the end of the Volcker era inflation risk was hence tilted to the downside. Subsequently, inflation risk jumped again to pre-Volcker levels before stabilizing around lower levels from roughly 1991, i.e. the end of the first Gulf war, to the financial crisis. This period is interrupted by two marked troughs in 1997 and 2002 that coincide with the Asian financial crisis and the burst of the dot-com bubble and subsequent recession, respectively. The financial crisis marks a turning point. Inflation risk decreased to historic lows, with risks being almost exclusively on the downside. Up until 2021 risks then remained subdued and tilted to the downside on average with peaks around 2011 and 2018 and a sharp decline from 2014 to 2016. Both peaks roughly align with periods in which energy prices increased, whereas the trough aligns with the oil and gas price plunge that lasted from 2014 to 2016. Finally, risk again fell during the pandemic before quickly increasing to historical highs in 2022.

Comparing the results to the corresponding estimates of the stochastic volatility and constant parameter model, a few differences emerge. For most of the sample, the estimates

are generally on par; however, the stochastic volatility model overstates inflation risks during the 90s and understates inflation risks during the recent high inflation period compared to the density regression model. Similarly, the constant volatility model suggest a balance of risk that is more tilted towards deflation pressures from the mid-80s up until the financial crisis and more pronounced deflation risks during the recession that followed the pandemic.

For $h = 4$ the results are generally comparable and the dynamics of BR are in line with those for $h = 1$, though they are less volatile. The main differences emerge in comparison with the stochastic volatility and constant parameter model. At $h = 4$, the SV model indicates substantially less inflation risk during the Volcker-era and the recent high inflation period. In addition, it suggests higher inflation risks leading up to the financial crisis compared the density regression model. Similar to before, the constant parameter model indicates more muted inflation risks to the upside and downside for most of the sample.

In practice most central bank communication rules out $\alpha = \beta = 0$ and instead implies $\alpha = \beta \geq 1$. To see this, consider the illustrative example in Kilian and Manganelli (2008). Assume that a central banker is faced with two scenarios, (a) 2.001% inflation with certainty or (b) 10% inflation with 20% probability and inflation less than 2% with 80% probability. If $\alpha = \beta = 0$, then (a) is worse, because $|BR_{0,0}^{(a)}| = |0.5| > |BR_{0,0}^{(b)}| = |-0.3|$. Undoubtedly, in practice central bankers would favour scenario (a) over (b) thus implying $\alpha > 0$ and $\beta > 0$. The right column of figure 2 hence shows the estimates for $\alpha = \beta = 2$. In this case, the risk measure corresponds to the target semi-variance and the central bank weights larger target deviations more strongly. As Kilian and Manganelli (2008) suggest, this specification is consistent with “low and stable inflation” and hence provides a useful benchmark.

With $\alpha = \beta = 2$, the overall picture is vastly different for $h = 1$. In part due to the change in scale, with these parameter settings, the BR seems less erratic and changes in inflation risk more persistent. From the early to mid 70s, the BR is strongly tilted to the upside before falling to lower levels between 1975 to 1978. In the left panel, inflation risk was elevated throughout the entire period. This suggests that the probability of missing the target was high, but the size of the expected target deviation decreased during this sub-sample. Until 1980 inflation risk reverted to its previous levels before decreasing to very low levels during the early 80s. Again, this period aligns well with the Volcker-era. Throughout the great moderation inflation risk remained generally subdued; however, a distinct peak coincides with the first Gulf war and a marked dip in inflation risk with the dot-com recession of 2002. Again, the financial crisis marks a turning point. After the

crisis, inflation risk was strongly on the downside before gradually normalizing. Up until the pandemic; however, deflation risk dominated slightly. Again, the oil and gas price plunge from 2014 to 2016 leaves a deflationary footprint. Finally, during the pandemic, the balance of risk tilts strongly to the downside, jumps back up to pre-financial crisis levels and then gradually increases for the rest of the sample, tilting increasingly to the upside. Because the only change compared to the left column is that the risk measure now takes preferences into account, this shows the amount of information that is obscured when considering purely statistical risk measures only.

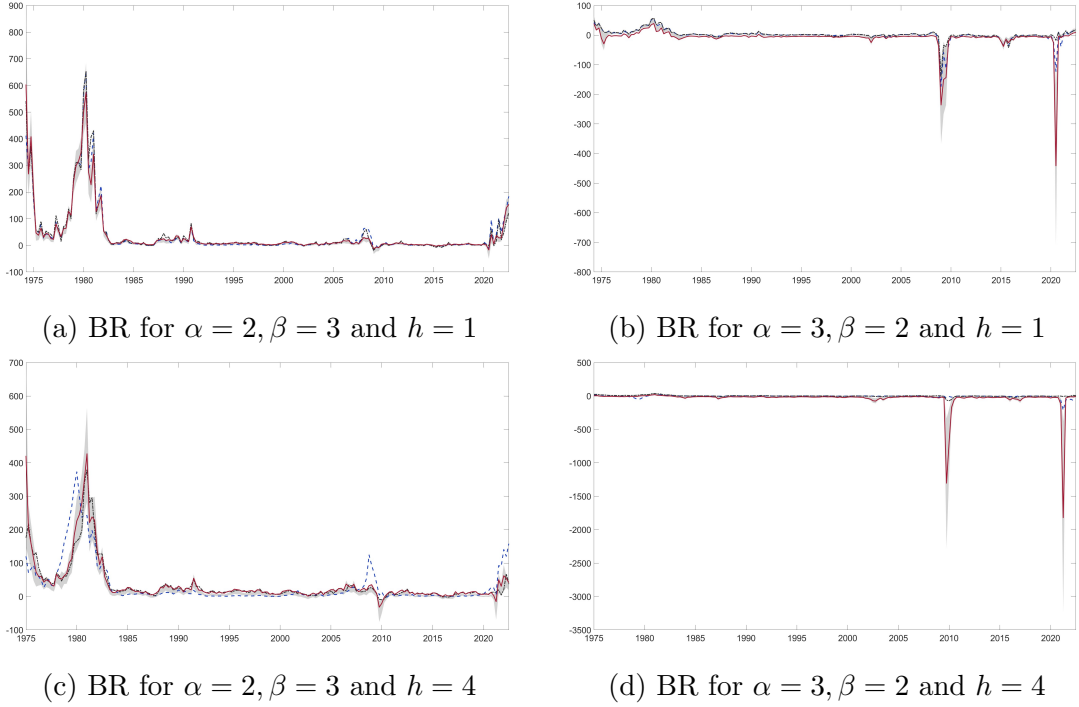
Comparing the results to the benchmark models overall confirms the previous picture. The dynamics are similar for most of the sample; however, the stochastic volatility model and the even more so the constant parameter model suggest higher inflation risks before the financial crisis and lower deflationary pressures during the great recession and the recession that followed the Covid-19 pandemic. Conversely, they also indicate lower inflation risks for most of the recent high inflation period.

As before, moving to $h = 4$ reduces the volatility of the balance of risk, but leaves the overall dynamics almost unaffected. Again, the differences to the benchmark models become increasingly visible. The stochastic volatility model diagnoses lower inflation risk during the Volcker-era and lower deflation risks during recessions. During the recent high inflation period, inflationary pressures are also understated compared to the density regression framework. In contrast, the constant parameter model tends to indicate higher inflation risks throughout the sample, but lower deflation risks during recessions.

As a second exercise, the analysis is repeated for asymmetric risk measures, that weight deflation risks more strongly than inflation risks and vice versa. These cases are illustrative, because central banks might e.g. be particularly cautious regarding deflationary pressure when interest rates are constrained by the effective lower bound. Similarly, central banks might be more concerned about further inflationary pressures, when inflation is already high and deflation risks seem generally muted. To illustrate such cases, Figure 3 contains the results for $\alpha = 2$ and $\beta = 3$ in the left column and the results for $\alpha = 3$ and $\beta = 2$ in the right column.

For preferences tilted towards inflation risks, the dynamics of the resulting risk measure are similar to $\alpha = \beta = 2$, albeit at an inflated scale and with deflation risks subdued at both forecast horizons. For $h = 1$ differences to the benchmark models emerge before the financial crisis and towards the end of the sample. At $h = 4$, these differences are again exaggerated. In particular, the stochastic volatility model suggest inflation risks to pick up earlier in the late 70s and more extreme inflation risk before the financial crisis and at the end of the sample.

Figure 3: The Balance of Risk



Notes: The solid red line indicates the MCMC estimate over the full sample obtained with the density regression model. The shaded area is the corresponding 86% credible interval. The dashed blue (dot-dashed black) line show the corresponding estimates computed with a model with stochastic volatility and constant volatility, respectively.

In the case of preferences tilted towards deflationary pressures, the general image is inverted. Inflationary pressures become subdued and deflationary pressures emphasized. For $h = 1$ this gives rise to lower inflation risks during the Volcker-era and at the end of the sample and more extreme deflation risks during recessions. Compared to the model proposed in this paper, the benchmark models generally indicate higher inflation risks and lower deflation risks during recessions. In case of $h = 4$, inflationary pressures become even more subdued, leaving the overall balance of risk dominated by deflation risk. In contrast to before, the constant parameter model now indicates no deflation risk during the recession that followed the pandemic and the stochastic volatility model implausibly suggests deflation risks during the post-Covid high inflation period. This likely results from the assumed symmetry of the inflation distribution. Unlike the density regression model, which allows for skewness, an increase in volatility increases probability mass equally to the left and right of the conditional mean. In extremely uncertain environments, the AR-SV model hence rarely predicts inflation/deflation risks exclusively.

6.3 Implied Policy Rates

As an additional validation exercise, it is illustrative to compute the policy rate that would minimize the balance of risk through the lens of the model. Assuming that the infinite horizon problem can be broken up into period-by-period problems, the implied policy rate is given by

$$\operatorname{argmin}_{i_t} \mathbb{E}(L_t), \text{ for } t = 1, 2, \dots \quad (17)$$

To keep the exercise in line with a medium-term policy objective, the loss function is set to $\mathbb{E}(L_t) = \sum_{h=1}^4 \delta^{h-1} BR_{t+h}$ for $\delta = (0, 1)$, i.e. the central bank minimizes the quarterly balance of risk accumulated over the next year and discounted with discount factor δ . In case of $\alpha = \beta = 2$, $w = 0.5$, and $\underline{\pi} = \bar{\pi}$, $BR_t = 0.5(\pi - \bar{\pi})^2$, the expected loss is minimized when the variance of inflation around the target is minimized (Kilian and Manganelli, 2007; Svensson, 1997).

In this case, the variance can in turn be directly obtained from the variance of the forecast distribution of the density regression model and is indirectly linked to the interest rate via the mixture weights and kernels. The minimization procedure hence repeatedly plugs in values for the interest rate at the current observation holding all other variables fixed, and then predicts the variance of the forecast distribution via the mixture model. The procedure terminates, once a value for i^* is found that minimizes the objective.

In practice, central banks tend to avoid extreme changes in the interest rate and instead pursue interest rate smoothing. To emulate this behavior, the loss function is augmented such that

$$\operatorname{argmin}_{i_t} w_i \cdot \sum_{h=1}^4 \delta^{h-1} BR_{t+h} + (1 - w_i) \cdot (i_t - \bar{i}_t)^2, \text{ for } t = 1, 2, \dots \quad (18)$$

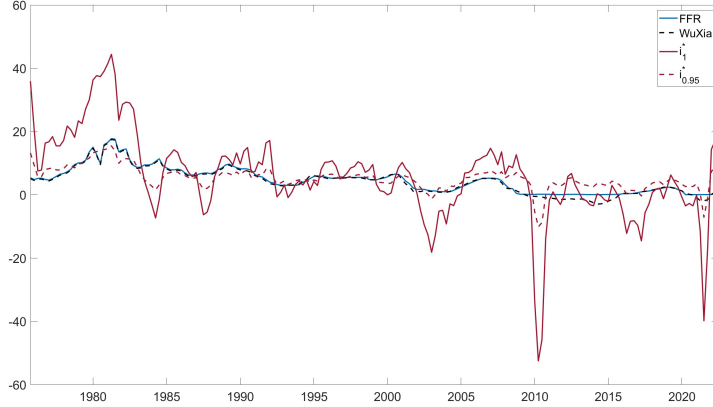
and the central bank also takes into account the volatility of the interest itself. Both implied interest rates with (dashed red) and without smoothing (red) are displayed in figure 4, together with the FFR (blue) and the shadow rate estimate in Wu and Xia (2016) (dashed black). w_i is calibrated, such that the volatility of the implied interest rate and the FFR are the same over the sample, resulting in $w_i = 0.96$. The procedure is detailed in appendix C.3.

Generally, the interest rates are highly correlated and follow the same dynamics.⁶ This implies, that the FED tends to change policy rates in the same direction as the model

⁶The correlation coefficient between the rate without (with) smoothing and the FFR is 0.704 (0.705).

proposed in this paper suggests on the back of a changing inflation risk outlook.

Figure 4: Implied Policy Rate Estimates



Notes: The blue line indicates the FFR and the dashed black line indicates the WuXia shadow rate. The red (dashed red) line indicates the policy rate without (with) interest rate smoothing that is implied by the risk measure obtained from the density regression model. The weight on smoothing is set such that the volatility of the predicted interest rate and the FFR are equal.

Zooming in, the implied policy rate without smoothing suggest large and implausible interest rate movements and largely exaggerates changes in the FFR, especially during booms and recessions. The smoothed implied policy rate; however, implies more reasonable rate setting. Compared to the FFR, it suggests slightly higher rates at the beginning of the sample, before the financial crisis, and low inflation period that followed the financial crisis. During the Volcker-era and great moderation, the rate overlaps with the actual FFR. Finally, it implies deeper interest rate cuts during recessions, such as the financial crisis (-10.1%) and pandemic (-7.1%), and more aggressive rate setting during the post-pandemic high inflation period (about 7.7%).

Overall, the risk measurement and modeling framework proposed in this paper, hence implies interest rate movements that are broadly in line with actual rate setting. At the same time, this suggest that the FED indeed considers inflation risks in its monetary policy framework.

Naturally, this exercise ignores other policy objectives and only considers the direct effect of interest rate changes, but ignores the indirect effect through changes in predictors. Further, the implied policy rates ignore the zero lower bound. The exercise should hence be interpreted through the lens of the model and inflation risks only and does not take a stance on optimal rate setting.

7 Analysing Drivers of Risk

Besides computing measures of risk, understanding the drivers of risk has been an active area of research. Examples include [Banerjee et al. \(2020\)](#); [Korobilis et al. \(2021\)](#); [Lopez-Salido and Loria \(2022\)](#); [Tagliabruni \(2020\)](#), who find that financial conditions drive especially downside inflation risks. The authors specify QR models and analyse these “risk factors” through the lens of extreme quantiles. This approach has a key drawback. Because the QRs are estimated independently, the risk factors remain local. In consequence, the results might differ strongly between e.g. the 90th and the 95th percentile. The drivers of risk are hence subject to the choice of the percentile level and do not generalize to other parts of the distribution. Conversely, approaches that link predictors to moments such as the conditional mean, variance, or skewness, only provide general information on the overall shape of the distribution. Changes in local probability mass remain obscured.

In the density regression approach, variables are linked to the full distribution of inflation, rather than moments or specific quantiles. This is, because they enter in the individual mixing probabilities and the mixing kernels. This allows to measure how individual predictors re-distribute probability mass dynamically across the entire conditional forecast distribution. Because the inflation risk measures are constructed directly from these densities, there is a mapping from the drivers of the forecast distribution to the drivers of the risk measures. Again, these fully take into account central bank preferences. This is important, because the central bank’s pricing of risk implies a preference based view on the drivers of risk. As an example, assume that in a given period the bottom tail of inflation is driven by a downturn in the domestic business cycle, but the top tail is driven by a spike in energy prices. If the central bank did not place any weight on downside risks, then the domestic business cycle should not emerge as a driver of risk. Based on this idea, this paper defines a driver of risk as in definition 7.1.

Definition 7.1 (*Contributions of Risk*)

A driver of downside risk at time t for horizon $t+h$ is a predictor, x_j , for which

$$\varphi_{t,j}^{DR_\alpha} = DR_{\alpha,t+h|t} - \mathbb{E}(DR_{\alpha,t+h}) - \sum_{i \in [1, \dots, n]: \neq j} \varphi_i^{DR_\alpha} < 0.$$

a driver of upside risk is a variable, j , for which

$$\varphi_{t,j}^{EIR_\beta} = EIR_{\beta,t+h|t} - \mathbb{E}(EIR_{\beta,t+h}) - \sum_{i \in [1, \dots, n]: i \neq j} \varphi_i^{EIR_\beta} > 0.$$

If $|\varphi_j| > |\varphi_i|$, for $i \neq j$, then variable x_j is a bigger risk factor at time t than variable x_i .

If $|\varphi_j| > |\varphi_i|$, for $i \neq j$, then variable x_j is a bigger risk factor at time t than variable x_i . A driver of downside (upside) risk is hence a variable that contributes negatively (positively) to deviations of the corresponding risk measure from the historical average. Unless the forecast distribution is tightly centred around the central bank target, there is always going to be some upside and downside risk. Expressing drivers in deviation from the historical average provides a simple normalization. In addition, these definitions imply efficiency, i.e. the individual contributions must add up to the value of the risk measure minus the historical average, and linearity, i.e. the contribution of any two predictors is the same as the sum of the individual contributions of the two predictors. This makes the contributions particularly easy to interpret.

Instead of looking at drivers of risk, it is also interesting to analyse how probability mass is re-distributed across $f_x(\pi)_{t+h|t}$. This provides a cross sectional view of risk and the drivers of the inflation forecast distribution. Definition 7.2 defines the contributions to the forecast density.

Definition 7.2 (*Contributions to the Forecast Distribution*)

Variable x_j is a driver of the forecast distribution at time t for horizon $t + h$ in the interval π_{i-1}^* to π_i^* , if

$$\varphi_j^{\pi_i^*} = \int_{\pi_{i-1}^*}^{\pi_i^*} f_x(\pi)_{t+h|t} d\pi - \int_{\pi_{i-1}^*}^{\pi_i^*} f_x(\pi)_{t+h} d\pi - \sum_{l \in [1, \dots, n]: l \neq j} \varphi_l^{\pi_i^*} \neq 0. \quad (19)$$

Again, these definitions imply efficiency and linearity. Under these assumptions, the individual contributions to the forecast distribution satisfy Lemma 7.1.

Lemma 7.1

Under definition 7.2 and given g grid points π^* , such that $\pi_{i-1}^* < \pi_i^*$, the contributions of the individual predictors preserve integrability, i.e.

$$\sum_{i=2}^g \left[\sum_j^n \varphi_j^{\pi_i^*} + \int_{\pi_{i-1}^*}^{\pi_i^*} f_x(\pi)_{t+h|t} d\pi \right] = \int_{-\infty}^{\infty} f_x(\pi)_{t+h|t} dx = 1.$$

The proof is given in appendix D.

As such, the contributions are comparable across time and grid point. A feature unique to the method proposed in this paper.

What has not been addressed so far, is how to estimate the individual contributions. A key challenge is that the individual variables enter the mixture components as well as the mixture weights. This implies interaction effects between the variables. As an example, an increase in variable x_j might lead to a change in the contribution of variable x_i , because the mixture weights change and hence the composition of the overall density. In addition, the risk measures are a non-linear function of the forecast density.

The explainable machine learning literature has proposed general approaches with desirable properties to deal with such cases. [Strumbelj and Kononenko \(2010\)](#) rephrase the problem as a cooperative game. Just like players in a cooperative game, variables in a forecasting model contribute to the model's final prediction. Adding a variable (player) to a model (game) that contains little additional information (contributes little additional skill) changes the prediction (pay-off) only slightly. The opposite is true for variables (players) that add a lot of information (skill). The key is; however, that game theory has established general solutions for attributing the pay-off in a cooperative game fairly to the players. These are the so-called Shapley values, pioneered by [Shapley \(1953\)](#). Let \mathbf{x} denote a set of variables. Following [Strumbelj and Kononenko \(2010\)](#) the Shapley value of variable x_j at time t for a model prediction \hat{f} can be written as

$$\varphi_j(\mathbf{x}_t; \hat{f}) = \sum_{\mathbf{x}' \subseteq \mathcal{C}(\mathbf{x}) \setminus \{k\}} \frac{|\mathbf{x}'|!(n - |\mathbf{x}'| - 1)!}{n!} [\hat{f}(x_j | \mathbf{x}' \cup \{k\}) - \hat{f}(x_j | \mathbf{x}')], \quad (20)$$

where \mathbf{x}' denotes a subset of \mathbf{x} , $|\mathbf{x}'|$ denotes its cardinality, $\mathcal{C}(\mathbf{x}) \setminus \{k\}$ is the set of all possible variable combinations upon excluding the j^{th} variable, and $\frac{|\mathbf{x}'|!(n - |\mathbf{x}'| - 1)!}{n!}$ is a combinatorial weight. In principle, equation 20 describes the weighted sum of the marginal contributions of variable x_j to model prediction \hat{f} in all possible coalitions.

In addition to efficiency and linearity, Shapley values possess additional useful axioms. Symmetry implies that variables with equal contributions have the same Shapley value, the dummy axiom implies that constants do not receive contributions, and monotonicity implies that Shapley values do not decrease, if a variable's contribution to the prediction does not decrease ([Strumbelj and Kononenko, 2010](#)).

In application, computing the contributions for all possible collocations at every point in time is computationally intensive and often infeasible. ([Strumbelj and Kononenko, 2010](#)) hence propose an approximation based on Monte Carlo sampling that provide accurate approximations under predictor independence. Based on this idea, this paper proposes two sampling algorithms for computing the contribution of variable x_j to the predictive density

of inflation in definition 7.2 and the risk measures in definition 7.1. The full algorithms are given by algorithm 3 and 4 in appendix B, respectively. Because computing contributions is particularly useful in applied policy work, the algorithms are fully adapted to real-time monitoring and out-of-sample forecasting exercises. In addition, the algorithms are universal in that their use extends beyond the model presented in this paper. As an example, algorithm 3 can also be used to decompose the forecast density generated with any other semi-parametric mixture model with trivial adjustments.

For one time period t and one variable j , both algorithms evolve as follows:

1. At given time period t , sample a random collocation, S , from $\mathcal{C}(x)$ and a random time period, t^* , from $1, \dots, t - 1$.
2. Replace the values in \mathbf{x}_t for the variables in S with the values in \mathbf{x}_{t^*} .
3. Create two vectors of observations. The first one contains x_j at time t , the other one also has $x_{j,t}$ replaced with x_{j,t^*} .
4. Compute the risk measure (predicted density) for both vectors. The difference yields the marginal contribution of x_j .
5. Repeat the procedure for a number of MC samples, M . The average of these marginal contribution gives a measure of $\varphi_{t,j}^{DR_\alpha}$ and $\varphi_{t,j}^{EIR_\beta}$ or $\varphi_j^{\pi^*}$.

Repeating the algorithm at different time periods and for different variables, x_j , then yields the full sequence of Shapley values for all variables. In theory, the computations can also be repeated at different MCMC draws or simulated posterior draws in the case of VB, to yield estimates of credible intervals and standard errors.

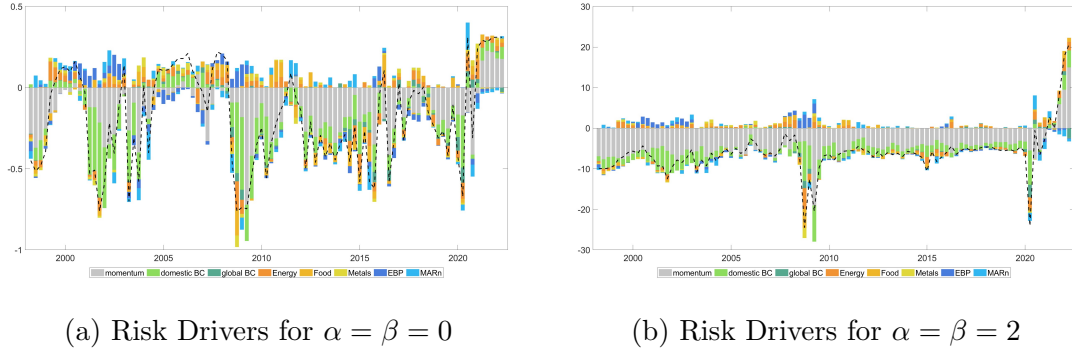
8 Empirical Drivers of Inflation Risk

8.1 Out-of-Sample Drivers of the Balance of Risk

In this section, the drivers of the balance of risk are computed, using the algorithms presented in section 7. Results for the individual upside and downside risk are shown in appendix E. The general setup is identical to the forecasting exercise presented earlier; however, for simplicity the focus is on $h = 1$, i.e. one quarter ahead annualized inflation. Results for other horizons are computed analogously. To obtain the results for objects such as annual inflation, in practice one can either change the forecasting target or aggregate

the quarterly forecasts and adjust the algorithms accordingly. Generally, note that the results should be interpreted through the lens of predictions and not be viewed as a fully structural exercise. Fully structural exercises are left for future research.

Figure 5: Drivers of the Balance of Risk



Notes: The coloured bars indicate the contribution of the corresponding variable to the balance of risk for the respective parameter setting. The dashed line indicates the observed value for the balance of risk minus the sample average.

The results for the balance of risk are presented in figure 5. The first row contains the decomposition for the out-of-sample period and parameter settings $\alpha = \beta = 0$ in the left panel. The right panel shows the corresponding results for $\alpha = \beta = 2$. All results are computed based on $M = 1000$, i.e. 1000 random collocation-time-period samples. To avoid clutter, the constant and the 4 lags of quarterly inflation are treated as one group labeled “momentum”. Generally, because of the linearity of the variable contributions, one can treat the variables as one group in the algorithm. In practice, instead of constructing \mathbf{x}_t^{+j} and \mathbf{x}_t^{-j} for a single variable j , the observations are instead replaced for the entire group. By computing the group contribution directly, computational demand is greatly reduced. In practice, this allows to compute contributions even for very large data sets, facilitating the use in applied work.

Starting with the left panel, the 1997 fall in predicted inflation risk is mostly driven by the domestic business cycle and falling commodity prices, abstracting from past dynamics. Monetary policy and credit spreads contribute positively, counteracting the deflationary forces. Subsequently, inflation risk increases above the historical level, mostly on the back of a recovery in the domestic business cycle as well as increasing commodity prices. The collapse of inflation risk following the burst of the dot-com bubble is predominantly driven by the recession and hence cooling of the domestic business cycle. At the same time, monetary policy and credit conditions again provide strong counteracting pressure,

as can be seen by the positive contributions to the balance of risks. This coincides well with the FED easing cycle that started in late 2000.

From 2004 onwards the domestic business cycle and increasing commodity prices tilt the balance of risk to the upside. Financial conditions contribute downward pressure, in line with FED tightening starting in late 2004. The energy price shocks observed during 2007 and 2008 also leave a marked footprint and drive the balance of risks upwards right before the financial crisis. Intuitively, at the beginning of the financial crisis, deflation risks are driven by mostly the domestic business cycle. Falling energy prices, monetary policy, and a contraction of global output provide additional downward pressure, whereas credit conditions stabilize the balance of risks. Subsequently, the balance of risk recovers supported by increasing commodity prices and by monetary policy. The increase in energy prices during this period correlates with the oil price shock of 2011, although the model attributes most weight to food prices.

The results for the low inflation period that lasted up until the pandemic are more mixed. Overall, the domestic and global business cycle contribute mostly deflationary pressures. Similarly, energy prices exert mostly downward pressure with the exception of the period around 2017 and 2018 that coincides with historic oil price increases. Finally, with the start of the pandemic and the introduction of restrictions, all predictors contribute deflationary pressures. The biggest drivers of downside risks; however, are the domestic and global business cycle. The subsequent recovery of inflation risk is largely driven by monetary policy, commodity prices, and to a lesser extend the business cycle. Towards the end of the sample, inflation risk can mostly be attributed to the domestic business cycle as well as increasing commodity prices. Monetary policy provides deflationary pressure. Even though this analysis is not structural, the results are very intuitive lending empirical support to the modelling approach.

As before, the right panel shows the results for $\alpha = \beta = 2$ and hence introduces risk aversion. The overall picture remains the same. At the beginning of the dot-com recession, the domestic business cycle and commodity prices contribute deflationary pressure that is counteracted by credit spreads. Subsequently, monetary policy, spreads and increasing commodity prices support the recovery. From roughly 2005 onwards, the domestic business cycle contributes inflation risk; however, the contributions are more muted compared to the left panel. Similarly, the decrease in the balance of risk at the start of the financial crisis is now roughly shared between the contraction of the domestic and global business cycle and a decline in commodity prices. Inflationary pressure is again exerted by credit spreads and monetary policy.

The low-inflation period until the pandemic differs slightly more from the left panel

and the contributions are less erratic. During this period, business cycle dynamics and commodity prices mostly drive deflationary pressures, with the exception of the 2015 and 2016 oil price surge, and monetary policy mostly drives inflationary pressures. At the start of the pandemic, the balance of risk again decreases mostly due to a contraction in the domestic and global business cycle. Compared to before, the following recovery in the balance of risks is now largely driven by monetary policy and the contribution of the domestic business cycle is more muted.

Additional differences emerge for the recent high inflation period towards the end of the sample. As the sample expands, monetary policy exerts increasing downward pressure. In addition, inflationary contributions of the domestic business cycle are now more pronounced than in the left panel. Intuitively, these differences in the relative contributions throughout the sample emerge, because the predictors shift probability mass differently across the predicted density. Because now the size of the target deviation impacts the balance of risk, a predictor that shifts mass to more extreme inflation realisations will contribute more than a predictor that shifts mass to lower realizations. This mechanism is illustrated in the next subsection. Overall, this result underlines that the CBs loss function not only influences the risk measure itself, but also the interpretation of the drivers of risk. Accounting for the pricing of risk is hence also crucial in this context.

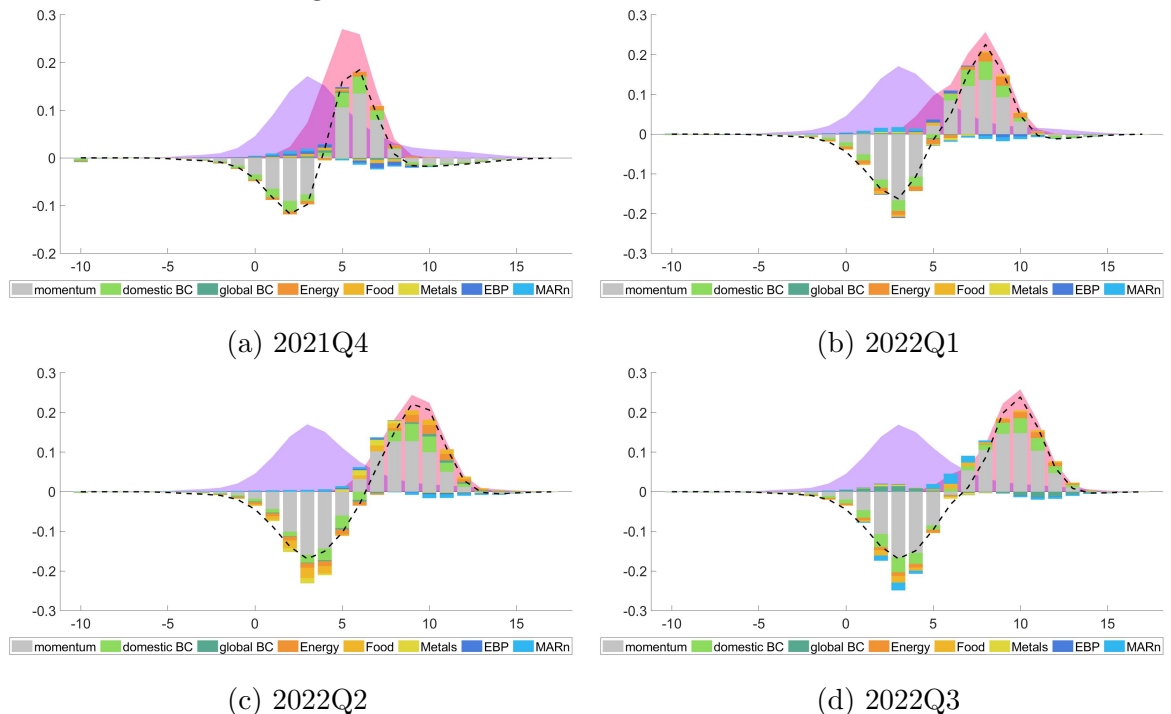
Finally, under risk aversion “momentum” almost exclusively contributes deflationary pressure over the entire sample. One reason is that the balance of risk was very high at the beginning of the sample and then decreased to lower levels up until the pandemic. In consequence, the average past balance of risk is decreasing as the sample expands and almost always higher than the predicted value, leading to a negative difference between the two. Because all contributions aggregate to this difference, they must compensate for the excess in historical inflation risk.

The definition of the risk measures has an additional advantage and provides a direct test for the accuracy of the proposed approximate algorithm. In particular, because the algorithms are based on sampling and do not explore all possible collocation-time-period combinations, in practice the contributions are not guaranteed to add up to the difference between the predicted balance of risk and the historical average. The latter is denoted by the black dashed lines in figure 5 and reproduced in figure 10 in the appendix together with the sum of all contributions. Overall, the algorithm works well. In the case of $\alpha = \beta = 0$, larger deviations only emerge in the period from ca. 2004 to 2006, around 2008, and 2018. In contrast, for $\alpha = \beta = 2$ the deviations are negligible over the entire sample.

8.2 Out-of-Sample Drivers of the Forecast Distribution

As pointed out above, in the proposed framework variables are linked to the entire forecast density, instead of moments. This unique feature allows to track how predictors shift probability mass dynamically across the forecast distribution of inflation. Throughout this section, the contributions are computed with algorithm 3, where $M = 1000$ and the density is discretized into one percentage point bins. Of course, in practice, e.g. a more finely spaced grid can be used at the expense of higher computational demand. Analogous to the previous section, all results are computed out-of-sample and the algorithms are re-run at every vintage. They are hence fully compatible with real-time applications in applied work.

Figure 6: Drivers of the Forecast Distribution



Notes: The purple density indicates the average historical density. The red density indicates the forecast density for 1-step ahead annualized quarterly inflation, estimated at the current vintage. The dashed black line indicates the difference between the predicted density and the historical average. The stacked bars contain the contributions.

The results are presented in figure 6. To keep things simple and illustrative, the focus is on the predictive out-of-sample densities for the last four quarters in the sample, i.e. 2021Q4 to 2022Q3. In each panel, the purple density denotes the historical average and

the red density indicates the predictive density for the respective quarter. Both densities are approximated over the same grid as the contributions to keep the picture consistent. As before, the variable contributions aggregate to the difference between the predicted density and the historical average, indicated by the black dashed line.

Starting with the top left panel, i.e. target quarter 2021Q4, the predicted density is less dispersed than the historical average and centred around higher inflation realizations. In addition, it is less fat-tailed and slightly negatively skewed. Zooming in on the variable contributions, abstracting from past dynamics, energy prices and the domestic business cycle are the biggest forces that move probability mass towards higher inflation realizations. Because the mass is moved to a more concentrated area, this contributes to a less dispersed forecast density. Food prices, monetary policy, credit spreads, and the global business cycle shift mass in the opposite direction. Overall, this gives rise to the slight negative skew.

Moving to the next quarter, the general pattern is the same; however, food prices emerge as an additional factor that shifts mass to the right, together with energy prices and the domestic business cycle. The overall effect is now stronger and mass is shifted to a larger interval compared to before, such that the forecast density becomes more dispersed and further shifts to the right. The effect of spreads and the interest rate remains similar to the left panel as both shift mass back to realizations in line with the 2% target. The global business cycle does not shift probability mass and remains neutral.

For the next quarter, 2022Q2, interesting changes emerge. Energy, food, and metal prices now shift increasingly much mass towards higher inflation and become by far the biggest driver. The effect of metal prices is more benign in that it shifts mass to less extreme realizations compared to food and energy prices. There is hence some heterogeneity across different commodity prices. In addition, compared to the previous quarters, both, the domestic and global business cycle shift probability mass to the right. This suggests that Global business cycle dynamics took slightly longer to pass through to the U.S. economy during the recent high inflation period. As a result, the predicted density shifts further to the right, whereas the dispersion remains similar.

For 2022Q3, the picture again changes. The effect of metal prices fades and the contribution of food and energy prices moderates slightly. The domestic business cycle continues to contribute to high inflation predictions by moving probability mass from lower to higher realization, but the effect is slightly smaller. In contrast, the global business cycle now shifts mass from very extreme realisations in the right tail of the distribution to the left tail and hence counteracts inflation pressures. The role of monetary policy is more ambiguous compared to before as it shifts mass from both, low realizations and

the right tail, towards the left tail of the forecast distribution. As such it contributes to negative skew in the overall forecast distribution, which remains centred around very high inflation.

9 Conclusion

This paper develops a joint framework to assess and monitor macroeconomic risk. The main advantages over existing approaches are that the proposed semi-parametric model accounts for the unknown, non-standard distribution of future inflation and allows the extraction of risk measures that are consistent with central bank preferences. To estimate the model, two algorithms, one MCMC algorithm for in-sample evaluations and an approximate VB algorithm that is particularly useful for forecasting and out-of-sample exercises. The conditionally Gaussian nature of the model allows the implementation without huge setup and estimation costs and facilitates the extension with different model formulations in applied work and academic research.

In addition, two simple and computationally fast algorithms are proposed that greatly enhance the interpretability of the resulting model output. The first algorithm decomposes the predicted risk measures into their underlying economic drivers, while preserving central bank preferences. This allows to evaluate the drivers of risk through the lens of the central bank’s pricing of risk. The second algorithm evaluates how economic covariates dynamically shift probability mass across the forecast distribution of inflation. Beyond this paper, this algorithm offers a tool to help interpret density forecasts generated with a broad range of mixture models, which are becoming increasingly popular in academic research and in practice.

The framework is evaluated on a set of empirical exercises. Compared to benchmark models, the model has properly calibrated PITs up to one year ahead and offers more precise point forecasts. In addition, the recent high-inflation period coincides with high inflation risk that is predominantly driven by the U.S. business cycle and commodity prices. At the same time, interest rates and credit spreads shift probability mass back towards on-target realizations of inflation hence providing a counteracting force.

Finally, although the focus is on inflation risk in these empirical exercises, the model can trivially be adjusted to other economic settings. One potential avenue for future research is the extension to a multivariate mixture model to dynamically estimate the joint distribution of key economic aggregates.

References

- ADRIAN, T., N. BOYARCHENKO, AND D. GIANNONE (2019): “Vulnerable Growth,” *American Economic Review*, 109, 1263–1289.
- ANDERSON, T. W. AND D. A. DARLING (1952): “Asymptotic Theory of Certain “Goodness of Fit” Criteria Based on Stochastic Processes,” *The Annals of Mathematical Statistics*, 23, 193–212.
- (1954): “A Test of Goodness of Fit,” *Journal of the American Statistical Association*, 49, 765–769.
- ANDREWS, D. W. K. (1993): “Tests for Parameter Instability and Structural Change With Unknown Change Point,” *Econometrica*, 61, 821–856.
- BANERJEE, R. N., J. CONTRERAS, A. MEHROTRA, AND F. ZAMPOLLI (2020): “Inflation at Risk in Advanced and Emerging Market Economies,” .
- BAUMEISTER, C. AND J. D. HAMILTON (2019): “Structural Interpretation of Vector Autoregressions with Incomplete Identification: Revisiting the Role of Oil Supply and Demand Shocks,” *American Economic Review*, 109, 1873–1910.
- BERKOWITZ, J. (2001): “Testing Density Forecasts, With Applications to Risk Management,” *Journal of Business & Economic Statistics*, 19, 465–474.
- BERNANKE, B. S. (2003): “Constrained Discretion and Monetary Policy,” *BIS Review*, 5, 1–8.
- BHATTACHARYYA, A., S. PAL, R. MITRA, AND S. RAI (2022): “Applications of Bayesian Shrinkage Prior Models in Clinical Research with Categorical Responses,” *BMC Medical Research Methodology*, 22, 126.
- BLANCHARD, O. J. AND B. S. BERNANKE (2023): “What Caused the US Pandemic-Era Inflation?” Tech. rep., National Bureau of Economic Research.
- BLEI, D. M., A. KUCUKELBIR, AND J. D. McAULIFFE (2017): “Variational Inference: A Review for Statisticians,” *Journal of the American Statistical Association*, 112, 859–877.
- BLINDER, A. S. (1997): “Distinguished Lecture on Economics in Government: What Central Bankers Could Learn from Academics—And Vice Versa,” *Journal of Economic Perspectives*, 11, 3–19.

- CARVALHO, C. M., N. G. POLSON, AND J. G. SCOTT (2010): “The Horseshoe Estimator for Sparse Signals,” *Biometrika*, 97, 465–480.
- CHERNOZHUKOV, V., I. FERNÁNDEZ-VAL, AND A. GALICHON (2010): “Quantile and Probability Curves Without Crossing,” *Econometrica*, 78, 1093–1125.
- CHRISTMAS, J. AND R. EVERSON (2011): “Robust Autoregression: Student-t Innovations Using Variational Bayes,” *IEEE Transactions on Signal Processing*, 59, 48–57.
- DE IORIO, M., P. MÜLLER, G. L. ROSNER, AND S. N. MAC EACHERN (2004): “An ANOVA Model for Dependent Random Measures,” *Journal of the American Statistical Association*, 99, 205–215.
- DE LA CRUZ-MESÍA, R., F. A. QUINTANA, AND P. MÜLLER (2007): “Semiparametric Bayesian Classification with Longitudinal Markers,” *Journal of the Royal Statistical Society, Series C* 56, 119–137.
- DOORNIK, J. A. AND H. HANSEN (2008): “An Omnibus Test for Univariate and Multivariate Normality*,” *Oxford Bulletin of Economics and Statistics*, 70, 927–939.
- DUNSON, D. B. AND J.-H. PARK (2008): “Kernel Stick-Breaking Processes,” *Biometrika*, 95, 307–323.
- FORBES, K. (2019): “Inflation Dynamics: Dead, Dormant, or Determined Abroad?” .
- FRÜHWIRTH-SCHNATTER, S. (2006): *Finite Mixture and Markov Switching Models*, Springer Series in Statistics, New York, NY: Springer.
- GELFAND, A. E., A. KOTTAS, AND S. N. MAC EACHERN (2005): “Bayesian Nonparametric Spatial Modeling With Dirichlet Process Mixing: Journal of the American Statistical Association: Vol 100, No 471,” *Journal of the American Statistical Association*, 100, 1021–1035.
- GEWEKE, J. AND M. KEANE (2007): “Smoothly Mixing Regressions,” *Journal of Econometrics*, 138, 252–290.
- GILCHRIST, S. AND E. ZAKRAJŠEK (2012): “Credit Spreads and Business Cycle Fluctuations,” *American Economic Review*, 102, 1692–1720.
- GOODFELLOW, I., Y. BENGIO, AND A. COURVILLE (2016): *Deep Learning*, MIT Press.

- GREENSPAN, A. (2004): “Risk and Uncertainty in Monetary Policy,” *American Economic Review*, 94, 33–40.
- GRIFFIN, J. E. AND M. F. J. STEEL (2006): “Order-Based Dependent Dirichlet Processes,” *Journal of the American Statistical Association*, 101, 179–194.
- GUTIÉRREZ, L., R. H. MENA, AND M. RUGGIERO (2016): “A Time Dependent Bayesian Nonparametric Model for Air Quality Analysis,” *Computational Statistics & Data Analysis*, 95, 161–175.
- ISHWARAN, H. AND L. F. JAMES (2001): “Gibbs Sampling Methods for Stick-Breaking Priors,” *Journal of the American Statistical Association*, 96.
- KILIAN, L. AND S. MANGANELLI (2007): “Quantifying the Risk of Deflation,” *Journal of Money, Credit and Banking*, 39, 561–590.
- (2008): “The Central Banker as a Risk Manager: Estimating the Federal Reserve’s Preferences under Greenspan,” *Journal of Money, Credit and Banking*, 40, 1103–1129.
- KOENKER, R. AND G. BASSETT (1978): “Regression Quantiles,” *Econometrica*, 46, 33.
- KOOP, G. AND D. KOROBILIS (2012): “Forecasting Inflation Using Dynamic Model Averaging*,” *International Economic Review*, 53, 867–886.
- (2023): “Bayesian Dynamic Variable Selection in High Dimensions,” *International Economic Review*, 64, 1047–1074.
- KOROBILIS, D. (2017): “Quantile Regression Forecasts of Inflation under Model Uncertainty,” *International Journal of Forecasting*, 33, 11–20.
- KOROBILIS, D., B. LANDAU, A. MUSSO, AND A. PHELLA (2021): “The Time-Varying Evolution of Inflation Risks,” *SSRN Electronic Journal*.
- KOROBILIS, D. AND K. SHIMIZU (2022): “Bayesian Approaches to Shrinkage and Sparse Estimation,” *Foundations and Trends® in Econometrics*, 11, 230–354.
- LOPEZ-SALIDO, D. AND F. LORIA (2022): “Inflation at Risk,” .
- MACHINA, MJ. AND M. ROTHSCHILD (1987): “Risk,” *The New Palgrave Dictionary of Economics*.
- MAKALIC, E. AND D. F. SCHMIDT (2016): “A Simple Sampler for the Horseshoe Estimator,” *IEEE Signal Processing Letters*, 23, 179–182.

- MCCRACKEN, M. AND S. NG (2020): “FRED-QD: A Quarterly Database for Macroeconomic Research,” .
- MIRANDA-AGRIPPINO, S. (2016): “Unsurprising Shocks: Information, Premia, and the Monetary Transmission,” .
- ORMEROD, J. T., C. YOU, AND S. MÜLLER (2017): “A Variational Bayes Approach to Variable Selection,” *Electronic Journal of Statistics*, 11, 3549–3594.
- POLSON, N. G., J. G. SCOTT, AND J. WINDLE (2013): “Bayesian Inference for Logistic Models Using Polya-Gamma Latent Variables,” *Journal of the American Statistical Association*, 108, 1339–1349.
- REICHLIN, L., G. RICCO, AND T. HASENZAGL (2020): “Financial Variables as Predictors of Real Growth Vulnerability,” .
- REN, L., L. DU, L. CARIN, AND D. B. DUNSON (2011): “Logistic Stick-Breaking Process,” *Journal of machine learning research : JMLR*, 12, 203–239.
- RIGON, T. AND D. DURANTE (2020): “Tractable Bayesian Density Regression via Logit Stick-Breaking Priors,” .
- RODRIGUES, A. AND D. B. DUNSON (2011): “Nonparametric Bayesian Models through Probit Stick-Breaking Processes - PMC,” *Bayesian Analysis*, 6, 145–178.
- ROSSI, B. AND T. SEKHPOSYAN (2014): “Evaluating Predictive Densities of US Output Growth and Inflation in a Large Macroeconomic Data Set,” *International Journal of Forecasting*, 30, 662–682.
- SHAPLEY, L. S. (1953): “A Value for N-Person Games,” .
- STOCK, J. AND M. WATSON (2010): “Modeling Inflation After the Crisis,” Tech. Rep. w16488, National Bureau of Economic Research, Cambridge, MA.
- STOCK, J. H. AND M. W. WATSON (1999): “Forecasting Inflation,” *Journal of Monetary Economics*, 44, 293–335.
- (2012): “Disentangling the Channels of the 2007-2009 Recession,” .
- STRUMBELJ, E. AND I. KONONENKO (2010): “An Efficient Explanation of Individual Classifications Using Game Theory,” *The Journal of Machine Learning Research*, 11, 1–18.

- SVENSSON, L. E. O. (1997): “Inflation Forecast Targeting: Implementing and Monitoring Inflation Targets,” *European Economic Review*, 41, 1111–1146.
- (2002): “Inflation Targeting: Should It Be Modeled as an Instrument Rule or a Targeting Rule?” *European Economic Review*, 46, 771–780.
- TAGLIABRACCI, A. (2020): “Asymmetry in the Conditional Distribution of Euro-area Inflation,” *SSRN Electronic Journal*.
- TUTZ, G. (1991): “Sequential Models in Categorical Regression,” *Computational Statistics & Data Analysis*, 11, 275–295.
- VILLANI, M., R. KOHN, AND P. GIORDANI (2009): “Regression Density Estimation Using Smooth Adaptive Gaussian Mixtures,” *Journal of Econometrics*, 153, 155–173.
- WEI, R. AND S. GHOSAL (2020): “Contraction Properties of Shrinkage Priors in Logistic Regression,” *Journal of Statistical Planning and Inference*, 207, 215–229.
- WU, J. C. AND F. D. XIA (2016): “Measuring the Macroeconomic Impact of Monetary Policy at the Zero Lower Bound,” *Journal of Money, Credit and Banking*, 48, 253–291.

A Estimation Algorithms

A.1 MCMC Sampler

This section presents the full algorithm for the MCMC sampler outlined in methodological section of the paper.

Algorithm 1: MCMC algorithm

```

[0] Initialize the model parameters.
begin
    [1] Assign each observation  $t = 1, \dots, T$  to a mixture component  $c = 1, \dots, C$ :
        for  $t = 1 : T$  do
            Sample  $G_t \in 1, \dots, C$  from a categorical distribution with probabilities
            
$$\text{pr}(G_t = c | -) = \frac{\left[ \nu_c(\mathbf{x}_t) \prod_{l=1}^{c-1} \{1 - \nu_l(\mathbf{x}_t)\} \right] \sqrt{\tau_c} [\sqrt{\tau_c} \{y_t - \mathbf{x}'_t \boldsymbol{\beta}_c\}]}{\sum_{q=1}^C \left[ \nu_q(\mathbf{x}_t) \prod_{l=1}^{q-1} \{1 - \nu_l(\mathbf{x}_t)\} \right] \sqrt{\tau_q} [\sqrt{\tau_q} \{y_t - \mathbf{x}'_t \boldsymbol{\beta}_q\}]},$$

            for every  $c = 1, \dots, C$ .
        end
    [2] Sample the parameters  $\psi_c$  and the horseshoe prior parameter  $\mathbf{v}_c$ ,  $\tau_c$ ,  $\eta_c$ , and  $\xi_c$  for each  $c = 1, \dots, C - 1$ :
        for  $c = 1, \dots, C - 1$  do
            [2a] Sample the parameters  $\psi_c$  for  $c = 1, \dots, C - 1$  exploiting the continuation-ratio parametrization
                and the results for Bayesian logistic regression in Polson et al. (2013):
                for  $t$  such that  $G_t > c - 1$  do
                    | Sample the Pólya-gamma distributed data  $\omega_{t,c}$  from  $(\omega_{t,c} | -) \sim PG(1, \mathbf{z}'_t \psi_c)$ .
                end
                Update  $\psi_c$  from  $(\psi_c | -) \sim N(\boldsymbol{\mu}_{\psi,c}, \boldsymbol{\Sigma}_{\psi,c})$  by Pólya-gamma augmentation, where
                 $\boldsymbol{\mu}_{\psi,c} = \boldsymbol{\Sigma}_{\psi,c} [\mathbf{X}' \boldsymbol{\kappa}_c]$ ,  $\boldsymbol{\Sigma}_{\psi,c} = [\mathbf{X}' \text{diag}(\omega_{1,c}, \dots, \omega_{\bar{T}_c,c}) \mathbf{X} + \tilde{\Upsilon}_c]^{-1}$ , with
                 $\boldsymbol{\kappa}_c = (\bar{z}_{1,c} - 0.5, \dots, \bar{z}_{\bar{T}_c,c} - 0.5)'$ ,  $\bar{z}_{t,c} = 1$  if  $G_t = c$  and  $\bar{z}_{t,c} = 0$  if  $G_t > c$ , and  $\tilde{\Upsilon}_c = \text{diag}(\bar{\tau}^{-2} \mathbf{v}_c^{-2})$ .
            [2b] Update the Horseshoe prior parameters following Makalic and Schmidt (2016) from:
                 $(v_{j,c}^2 | -) \sim IG\left(1, \frac{\psi_{j,c}^2}{2\bar{\tau}_c^2} + \frac{1}{\eta_{j,c}}\right)$ ,  $(\eta_{j,c} | -) \sim IG\left(1, 1 + \frac{1}{\lambda_{j,c}^2}\right)$ 
                 $(\bar{\tau}_c^2 | -) \sim IG\left(\frac{K+1}{2}, \frac{1}{\xi_c} + \sum_{j=1}^k \frac{\psi_{j,c}^2}{2v_{j,c}^2}\right)$ ,  $(\xi_c | -) \sim IG\left(1, 1 + \frac{1}{\bar{\tau}_c^2}\right)$ .
        end
    [3] Sample the parameters  $\boldsymbol{\beta}_c$  from  $(\boldsymbol{\beta}_c | -) \sim N(\boldsymbol{\mu}_{\beta_c}, \boldsymbol{\Sigma}_{\beta_c})$ , where
         $\boldsymbol{\mu}_{\beta_c} = \boldsymbol{\Sigma}_{\beta_c} (\tau_c \mathbf{X}'_c \mathbf{y}_c + \boldsymbol{\Sigma}_{\beta}^{-1} \boldsymbol{\mu}_{\beta})$ ,  $\boldsymbol{\Sigma}_{\beta_c} = (\tau_c \mathbf{X}'_c \mathbf{X}_c + \boldsymbol{\Sigma}_{\beta}^{-1})^{-1}$ .  $\mathbf{X}_c$  and  $\mathbf{y}_c$  correspond to the observations
        for which  $G_t = c$ .
    [4] Draw the precision parameter  $\tau_c$  for  $c = 1, \dots, C$ :
        for  $c = 1, \dots, C$  do
            | Sample  $\tau_c$  from  $(\tau_c | -) \sim G\left(a_\tau + \frac{1}{2} \sum_{t=1}^T \mathbb{I}(G_t = c), b_\tau + \frac{1}{2} \sum_{t:G_t=c} \{y_t - \mathbf{x}'_t \boldsymbol{\beta}_c\}^2\right)$ 
        end
    end

```

A.2 Variational Bayes Inference

Variational Bayes (VB) and MCMC both provide approximations to a given posterior. However; while MCMC relies on sampling, VB approximates the posterior through solving an optimization problem. For a general introduction to VB see Blei et al. (2017). Because this optimization problem requires fewer iterations than sampling from an

MCMC chain, VB's main advantage lies in its computational speed. As a caveat, whereas MCMC guarantees exact draws from the posterior, VB yields a solution close to the posterior. As such, VB is particularly useful for tasks where computational time is critical and accurate parameter estimates are less of a concern, such as, big-data problems, models with highly intractable posteriors, real-time monitoring tasks, or forecasting exercises. The algorithm proposed in this paper extends the VB algorithm in Rigon and Durante (2020) and introduces shrinkage into the sequential logistic regressions.

The algorithm evolves as follows:

1. Update the variational density of the mixture component assignment indicators ζ_{tc} . Here the model is augmented using the binary indicators z instead of the mixture component membership indicators G_t . This step differs from the MCMC sampler and follows Rigon and Durante (2020)
2. Update the variational densities corresponding to the regression coefficients in the logistic regressions, ψ_c , for all mixture components.
3. Update the variational density of the horseshoe prior coefficients. This step differs slightly from the MCMC sampler in that the horseshoe prior is parametrized differently.
4. Update the variational density of the Pólya-Gamma indicators ω_{tc} .
5. Update the variational density of the regression coefficients, β_c , and the precision parameters, τ_c , of the individual mixture components.

Throughout lower case letters denote scalars, bold lower case letters denote vectors and bold capital letters denote matrices. To ease notation, whenever indices referring to the mixture assignment indicators, time periods, or variables are suppressed, they are collected in a single vectors. Collect all model parameters in $\Theta = (\beta, \tau, z, \psi, \omega, \nu, \bar{\tau}^2, \eta, \xi)$. For a family of tractable densities $q(\Theta)$, we aim to find a density q^* that best approximates the posterior $p(\Theta|x)$ by minimizing

$$q_x^*(\Theta) = \operatorname{argmin}_{q \in \mathcal{Q}} \mathbb{D}_{KL}(q(\Theta||p(\Theta|x)). \quad (21)$$

This is equivalent to maximizing

$$ELBO = \mathbb{E}_{q_x(\Theta)} [\log p(\mathbf{x})] + \mathbb{E}_{q_x(\Theta)} [\log p(\Theta)] - \mathbb{E}_{q_x(\Theta)} [\log q_x(\Theta)], \quad (22)$$

where KL denotes the Kullback-Leibler divergence. Importantly, the solution requires optimizing over a family of distribution functions and hence the application of variational calculus. A key part of VB is to simplify the variational posterior by factorization, such that the resulting optimization problem becomes tractable. On the one hand, the simpler the resulting posterior, the easier the optimization problem. On the other hand, this implies independence assumptions between the individual variational components and hence leads to approximation error. This gives rise to a trade-off (Ormerod et al., 2017). In the proposed estimator, I apply the so-called mean-field factorization. This yields

$$\begin{aligned} q_x(\Theta) &= \prod_{c=1}^{C-1} q_x(\boldsymbol{\psi}_c) \prod_{c=1}^{C-1} q_x(\xi_c) \prod_{c=1}^{C-1} \prod_{j=1}^n q_x(\nu_{j,c}^2) \prod_{c=1}^{C-1} \prod_{j=1}^n q_x(\bar{\tau}_{j,c}^2) \prod_{c=1}^{C-1} \prod_{j=1}^n q_x(\eta_{j,c}^2) \\ &\cdot \prod_{c=1}^C q_x(\beta_c) \prod_{c=1}^C q_x(\tau_c) \prod_{c=1}^{C-1} \prod_{t=1}^T q_{x_t}(z_{tc}) \prod_{c=1}^{C-1} \prod_{t=1}^T q_{x_t}(\omega_{tc}). \end{aligned} \quad (23)$$

This implies independence between the regression coefficients in the logistic regressions and kernel regressions, the cluster assignment indicators, the parameters of the horseshoe prior, and the Pólya-Gamma indicators. Additionally, I assume that the priors are conditionally independent.

Given these assumptions, the solution to the optimization problem can be obtained by sequentially iterating over the densities

$$q_x(\Theta_l) \propto \exp \mathbb{E}_{q_x(\Theta_{(-l)})} (\log p(\Theta_l | \Theta_{(-l)}, \mathbf{x})) \quad (24)$$

where $\Theta_{(-l)}$ denotes all elements of Θ , excluding those in the l^{th} group, $l = 1, \dots, L$.

As a result, the variational posterior can be obtained by calculating the variational expectation of the conditional posterior. As described above, the accuracy of the variational approximation hinges on how well the partitioning matches the independence structure of the parameters in the target posterior. For a general discussion of this issue see e.g. Ormerod et al. (2017). To arrive at the final variational densities, I insert 23 and the priors into 24. The final algorithm is given in algorithm 2.

Finally, note that I used a different parametrization of the horseshoe prior in deriving the algorithm:

$$\psi_c | \{\nu_{j,c}^2, \eta_{j,c}, \bar{\tau}_{j,c}^2\}_{j=1}^n, \xi_c \sim N(\mathbf{0}, \boldsymbol{\Lambda}_c), \quad (25)$$

$$\begin{aligned}\bar{\lambda}_{j,c}^2 | v_{j,c} &\sim G^{-1} \left(\frac{1}{2}, \frac{1}{v_{j,c}} \right), \quad \text{for } j = 1, \dots, n, \\ v_{j,c} | \bar{\tau}_{j,c}^2 &\sim G^{-1} \left(\frac{1}{2}, \frac{1}{b_\psi^2 \bar{\tau}_{j,c}^2} \right), \quad \text{for } j = 1, \dots, n, \\ \bar{\tau}_{j,c}^2 | \xi_c &\sim G^{-1} \left(\frac{1}{2}, \frac{1}{\xi_c} \right), \\ \xi_c &\sim G^{-1} \left(\frac{1}{2}, 1 \right),\end{aligned}$$

where b_ψ is a hyperparameters, which I set to 0.0001 in application.

Algorithm 2: Variational Bayes algorithm

[0] Initialize the model parameters. Let $q^m(\cdot)$ denote a generic variational distribution at iteration m.

begin

- [1] Compute the variational density $q_{\mathbf{x}_t}^*(z_{ic})$ for each $t = 1, \dots, T$ and $c = 1, \dots, C - 1$:
- for** $t = 1 : T$ **do**
- for** $c = 1 : C$ **do**
- Following Rigon and Durante (2020), $q_{x_t}^*(z_{ih})$ coincides with the probability mass function of $Bern(\rho_{ih})$, where
- $$\rho_{ih} = \frac{1}{1 + exp\left(-\left[\mathbf{x}_t' \mathbf{\Xi}(\phi_c) + \sum_{l=1}^C \zeta_{tl}^c (0.5 \cdot \mathbb{E}(\log \tau_l) - 0.5 \cdot \mathbb{E}(\log \tau_l) \cdot \mathbb{E}(y_t - \mathbf{x}_t' \boldsymbol{\beta}_l)^2)\right]\right)}.$$
- with $\zeta_{tl}^c = \prod_{r=1}^{l-1} (1 - \rho_{tr})$ for $l = c$ and $\zeta_{tl}^c = -\rho_{tl} \prod_{r=1, r \neq c}^{l-1} (1 - \rho_{tr})$, and $\rho_{tC} = 1$.
- Assign:** $\mathbb{E}(\zeta_{tc}) = \mathbb{E}\left(z_{tc} \prod_{l=1}^{c-1} (1 - z_{tl})\right) = \rho_{tc} \prod_{l=1}^{c-1} (1 - \rho_{tl})$, and $\mathbb{E}(z_{tc}) = \rho_{tc}$.
- end**
- end**
- [2] Update $q_x^*(\psi_c)$ and $q_x^*(\mathbf{v}_c^2)$, $q_x^*(\bar{\tau}_c^2)$, $q_x^*(\boldsymbol{\eta}_c)$, and $q_x^*(\xi_c)$ for $c = 1, \dots, C - 1$:
- for** $c = 1, \dots, C - 1$ **do**
- [2a] Update $q_x^*(\psi_c)$ from $N(\boldsymbol{\mu}_{\psi,c}, \boldsymbol{\Sigma}_{\psi,c})$, with $\boldsymbol{\Sigma}_{\psi,c} = (\mathbf{X}' \mathbf{V}_c \mathbf{X} + \boldsymbol{\Lambda}^{-1})^{-1}$, $\boldsymbol{\mu}_{\psi,c} = \boldsymbol{\Sigma}_{\psi,c} (\mathbf{X}' \boldsymbol{\kappa}_c)$, with $\boldsymbol{\kappa}_c = (\mathbb{E}(z_{1,c}) - 0.5, \dots, \mathbb{E}(z_{T,c}) - 0.5)'$, $\mathbf{V}_c = diag(\mathbb{E}(\omega_{1c}), \dots, \mathbb{E}(\omega_{Tc}))$, and $\boldsymbol{\Lambda}_c^{-1} = diag(\mathbb{E}(\mathbf{v}_c^2) \mathbb{E}(\bar{\tau}_c^2))$.
- Assign:** $\mathbb{E}(\psi_c) = \boldsymbol{\mu}_{\psi,c}$ and $\mathbb{E}(\psi_c^2) = \boldsymbol{\mu}_{\psi,c}^2 + diag(\boldsymbol{\Sigma}_{\psi,c})$.
- [2b] Update $q_x^*(\mathbf{v}_c^2)$, $q_x^*(\bar{\tau}_c^2)$, $q_x^*(\boldsymbol{\eta}_c)$, and $q_x^*(\xi_c)$ for $c = 1, \dots, C - 1$:
- $$q_x^*(\mathbf{v}_{j,c}^2) = IG(a_{v,c}, b_{v,c}) = IG\left(1, \frac{\mathbb{E}(\psi_{j,c}^2)}{2} + \mathbb{E}\left(\frac{1}{\eta_{j,c}}\right)\right),$$
- $$q_x^*(\eta_{j,c}) = IG(a_{\eta,c}, b_{\eta,c}) = IG\left(1, \mathbb{E}\left(\frac{1}{v_{j,c}^2}\right) + b_{\psi}^{-2} \mathbb{E}\left(\frac{1}{\bar{\tau}_{j,c}^2}\right)\right),$$
- $$q_x^*(\bar{\tau}_{j,c}^2) = IG(a_{\bar{\tau},c}, b_{\bar{\tau},c}) = IG\left(1, b_{\psi}^{-2} \mathbb{E}\left(\frac{1}{\eta_{j,c}}\right) + \mathbb{E}\left(\frac{1}{\xi_c}\right)\right),$$
- $$q_x^*(\xi_c) = IG(a_{\xi,c}, b_{\xi,c}) = IG\left(\frac{n+1}{2}, 1 + \sum_{j=1}^n \mathbb{E}\left(\frac{1}{\bar{\tau}_{j,c}^2}\right)\right),$$
- for $j = 1, \dots, n$.
- Assign:** $\mathbb{E}(\mathbf{v}_{j,c}^2) = \frac{a_{v,c}}{b_{v,c}}$, $\mathbb{E}(\eta_{j,c}) = \frac{a_{\eta,c}}{b_{\eta,c}}$, $\mathbb{E}(\bar{\tau}_{j,c}^2) = \frac{a_{\bar{\tau},c}}{b_{\bar{\tau},c}}$, and $\mathbb{E}(\xi_c) = \frac{a_{\xi,c}}{b_{\xi,c}}$.
- end**
- end**
- [3] Update $q_x^*(\omega_{tc})$ for $t = 1, \dots, T$ and $c = 1, \dots, C$.
- for** $t = 1 : T$ **do**
- for** $c = 1 : C$ **do**
- Update $q_x^*(\omega_{tc}) \sim PG(1, \delta_{tc})$, with $\delta_{tc}^2 = \mathbf{x}_t' \mathbf{\Xi}(\psi_c^2) \mathbf{x}_t$.
- Assign:** $\mathbb{E}(\omega_{tc}) = 0.5 \cdot \delta_{tc}^{-1} \tanh(0.5 \cdot \delta_{tc})$.
- end**
- end**
- [4] Update $q_x^*(\boldsymbol{\beta}_c)$ and $q_x^*(\tau_c)$ for $c = 1, \dots, C$:
- for** $c = 1 : C$ **do**
- Update $q_x^*(\boldsymbol{\beta}_c) \sim N(\boldsymbol{\mu}_{\beta,c}, \boldsymbol{\Sigma}_{\beta,c})$ and $q_x^*(\tau_c) \sim IG(a_{\tau_c}, b_{\tau_c})$, with $\boldsymbol{\Sigma}_{\beta,c} = (\mathbf{X}' \boldsymbol{\Gamma}_c \mathbf{X} + \boldsymbol{\Sigma}_{\beta}^{-1})^{-1}$, $\boldsymbol{\mu}_{\beta,c} = \boldsymbol{\Sigma}_{\beta,c} (\mathbf{X} \boldsymbol{\Gamma}_c \mathbf{y} + \boldsymbol{\Sigma}_{\beta}^{-1} \boldsymbol{\mu}_{\beta})$, $a_{\tau_c} = a_{\tau} + 0.5 \sum_{t=1}^T \mathbb{E}(\zeta_{tc})$, and $b_{\tau_c} = b_{\tau} + 0.5 \sum_{t=1}^T \mathbb{E}(\zeta_{tc}) \mathbb{E}((y_t - \mathbf{x}_t' \boldsymbol{\beta}_c)^2)$, with $\boldsymbol{\Gamma}_c = \mathbb{E}(\tau_c) diag(\mathbb{E}(\zeta_{tc}), \dots, \mathbb{E}(\zeta_{Tc}))$.
- Assign:** $\mathbb{E}(\boldsymbol{\beta}_c) = \boldsymbol{\mu}_{\beta,c}$, $\mathbb{E}(\boldsymbol{\beta}_c^2) = \boldsymbol{\mu}_{\beta,c}^2 + diag(\boldsymbol{\Sigma}_{\beta,c})$, and $\mathbb{E}(\tau_c) = \frac{a_{\tau_c}}{b_{\tau_c}}$.
- end**
- end**

B Algorithms for Computing Drivers of Risk

This section gives the full algorithms for computing the drivers of risk and the forecast distribution, as detailed in the main body of the manuscript.

Algorithm 3: Risk Measure Shapley Values

```

[0] Specify the number of samples  $M$ , and set  $\alpha, \beta, \bar{\pi}, \underline{\pi}$ .
[1] Compute the contribution for variable  $j$  to the risk measures for  $t + h$  at time  $t$ .
begin
    [a] Iterate over random samples. The sampling population is the set of all time-period/variable permutation pairs.
        for  $m = 1 : M$  do
            [i] Sample a random time period,  $t^* \in_R [1 : t - 1]$ , from the preceding sample of observations and set  $\mathbf{z}_t = \mathbf{x}_{t^*}$ .
            [ii] Choose a random permutation of variables,  $S$ , i.e. sample  $S \subseteq_R [1, \dots, j - 1, j + 1, \dots, n]$ , where  $|S| \leq n - 1$ .
            [iii] Create two new data vectors. For the first vector, replace the values in  $\mathbf{x}_t$  with the values in  $\mathbf{z}_t$  for the indices in  $S$ . For the second vector, also replace  $x_{t,j}$  with  $z_{t,j}$ . As an example, let  $S = [1, j + 1, \dots, j + n]$ . This yields:
                
$$\mathbf{x}_t^{+j} = [z_{t,1}, x_{t,2}, \dots, x_{t,j-1}, x_{t,j}, z_{t,j+1}, \dots, z_{t,n}]$$

                
$$\mathbf{x}_t^{-j} = [z_{t,1}, x_{t,2}, \dots, x_{t,j-1}, z_{t,j}, z_{t,j+1}, \dots, z_{t,n}].$$

            [iv] Compute the contribution for  $j$  to  $DR_\alpha$  and  $EIR_\beta$  at draw  $m$ .
                
$$V_{m,j}^{DR_\alpha} = - \left( \int_{-\infty}^{\underline{\pi}} (\underline{\pi} - \pi)^\alpha f_x(\pi)_{t+h|t}^{+j} d\pi - \int_{-\infty}^{\underline{\pi}} (\pi - \bar{\pi})^\alpha f_x(\pi)_{t+h|t}^{-j} d\pi \right)$$

                
$$V_{m,j}^{EIR_\beta} = \int_{\bar{\pi}}^{\infty} (\underline{\pi} - \pi)^\beta f_x(\pi)_{t+h|t}^{+j} d\pi - \int_{\bar{\pi}}^{\infty} (\pi - \bar{\pi})^\beta f_x(\pi)_{t+h|t}^{-j} d\pi$$

        end
    [b] Compute the contribution of  $j$  to  $DR_\alpha$  and  $EIR_\beta$ ,  $\hat{\varphi}_j^{DR_\alpha}$  and  $\hat{\varphi}_j^{EIR_\beta}$ , by taking the average over all samples,  $M$ .
        
$$\hat{\varphi}_j^{DR_\alpha} = \frac{1}{M} \sum_m V_{m,j}^{DR_\alpha} \text{ and } \hat{\varphi}_j^{EIR_\beta} = \frac{1}{M} \sum_m V_{m,j}^{EIR_\beta}.$$

end

```

Notes: \subseteq_R and \in_R denote a random subset and random element, respectively. The integrals can be computed with quadrature methods.

Algorithm 4: Forecast Density Shapley Values

[0] Specify the number of samples M , and the number of grid points, g . Generate a grid for $\hat{\pi}$, with $\hat{\pi}_i \in [\lfloor \pi_{1:T} \rfloor, \dots, \lceil \pi_{1:T} \rceil]$ for $i = 1, \dots, g$.

[1] Compute the contribution for variable j to the forecast distribution for $t + h$ at time t .

begin

- [a] Iterate over random samples. The sampling population is the set of all time-period/variable permutation pairs.
- for** $m = 1 : M$ **do**

 - [i] Sample a random time period, $t^* \in_R [1 : t - 1]$, from the preceding sample of observations and set $\mathbf{z}_t = \mathbf{x}_{t^*}$.
 - [ii] Choose a random permutation of variables, S , i.e. sample $S \subseteq_R [1, \dots, j - 1, j + 1, \dots, n]$, where $|S| \leq n - 1$.
 - [iii] Create two new data vectors. For the first vector, replace the values in \mathbf{x}_t with the values in \mathbf{z}_t for the indices in S . For the second vector, also replace $x_{t,j}$ with $z_{t,j}$. As an example, let $S = [1, j + 1, \dots, j + n]$. This yields:

$$\mathbf{x}_t^{+j} = [z_{t,1}, x_{t,2}, \dots, x_{t,j-1}, x_{t,j}, z_{t,j+1}, \dots, z_{t,n}]$$

$$\mathbf{x}_t^{-j} = [z_{t,1}, x_{t,2}, \dots, x_{t,j-1}, z_{t,j}, z_{t,j+1}, \dots, z_{t,n}].$$
- [iv] Compute the contribution for j between the grid points $\hat{\pi}_i$ and $\hat{\pi}_{i-1}$ at draw m

$$V_{m,j}^i = \int_{\hat{\pi}_{i-1}}^{\hat{\pi}_i} f_x(\pi)_{t+h|t}^{+j} d\pi - \int_{\hat{\pi}_{i-1}}^{\hat{\pi}_i} f_x(\pi)_{t+h|t}^{-j} d\pi \quad \text{for every } i = 2, \dots, g.$$

end

[b] Compute the contribution of j between grid points $\hat{\pi}_i$ and $\hat{\pi}_{i-1}$, $\hat{\varphi}_j^i$, by taking the average over all samples, M .

$$\hat{\varphi}_j^i = \frac{1}{M} \sum_m^M V_{m,j}^i.$$

end

Notes: \subseteq_R and \in_R denote a random subset and random element, respectively. The integrals can be computed with quadrature methods.

C Additional Algorithms

C.1 Computing Quantiles

By the properties of the normal distribution, the sum of multiple normals is again normal. The CDF and PDF are hence available as the sum of the appropriately reweighted individual mixture components, as shown above. However, this convenient property does not hold for the quantile function. An analytical solution is hence not available and I device a simple root finding procedure, where

$$\Phi_x(\pi_{t+h})|_{\hat{Q}_x^\tau(\pi_{t+h})} - \tau = 0, \quad (26)$$

where τ denotes a percentile of interest and $\Phi_x(\pi_{t+h})$ denotes the CDF of the mixture model that is evaluated at a candidate solution $\hat{Q}_x^\tau(\pi_{t+h})$. The desired percentile, $Q_x^\tau(\pi_{t+h})$, is the solution to Equation (26). Note that because the CDF is proper and we estimate the entire distribution simultaneously, the resulting conditional quantiles do not cross. This is an advantage compared to univariate quantile regressions models.

C.2 Computing the Optimal Number of Mixture Components

As mentioned above, the performance of the mixture model also hinges on the truncation point of the infinite sum of mixture components. Especially in forecasting exercises, it might hence be useful to select this truncation point automatically. In the Bayesian context, the marginal data likelihood allows to solve this model selection problem; however the computation of the marginal likelihood is usually computationally cumbersome. In the context of Variational Bayes, the ELBO, i.e. the convergence criterion of the optimization problem, provides an accurate approximation of the marginal likelihood. Because the algorithm is computationally fast, solving the model selection problem with VB is hence an ideal alternative. This gives rise to the following algorithm:

1. Set an upper bar on the number of mixture components \bar{C} .
2. For $C = 1, \dots, \bar{C}$, re-estimate the model with VB and store the ELBO.
3. Set

$$C^* = \arg \max_C ELBO_C.$$

4. Re-estimate/store the estimates for the model estimated with C^* .

Because the algorithm is fast, this optimization can even be repeated in real-time at every new data vintage, provided \bar{C} is not too large. I recommend $\bar{C} = 5$ or $\bar{C} = 10$.

C.3 Calibrating the Degree of Interest Rate Smoothing

This section details the procedure for computing the implied policy rate with interest rate smoothing:

1. Set up a grid for $w_i \in [0, 1]$.
2. Compute the implied policy rate path and its variance over the full sample for each grid point.
3. Collect all variances for all paths under different grid points and subtract the variance of the FFR.
4. Interpolate the resulting curve. This results in a monotonically increasing curve with a single root.
5. Run a root finding procedure to find the w_i that results in an implied interest rate that has the same variance as the FFR over the full sample.

D Proof

D.1 Proof of Lemma 7.1

Proof: Let $f_x(\pi)_{t+h|t}$ denote the forecast distribution of inflation at time t for horizon $t+h$.

Further, let π^* denote a set of g ordered grid points across the entire support of π . π_i^* and π_{i-1}^* hence denote two neighbouring grid points such that $\pi_{i-1}^* < \pi_i^*$. Further, let $\pi_1^* = -\infty$ and $\pi_g^* = \infty$. Then

$$\int_{-\infty}^{\infty} f_x(\pi)_{t+h|t} dx = \sum_{i=2}^g \int_{\pi_{i-1}^*}^{\pi_i^*} f_x(\pi)_{t+h|t} dx = 1$$

Analogously,

$$\int_{-\infty}^{\infty} f_x(\pi)_{t+h} dx = \sum_{i=2}^g \int_{\pi_{i-1}^*}^{\pi_i^*} f_x(\pi)_{t+h} dx = 1.$$

Given the definition of the predictor contributions

$$\sum_j^n \varphi_j + \int_{\pi_{i-1}^*}^{\pi_i^*} f_x(\pi)_{t+h} d\pi = \int_{\pi_{i-1}^*}^{\pi_i^*} f_x(\pi)_{t+h|t} dx.$$

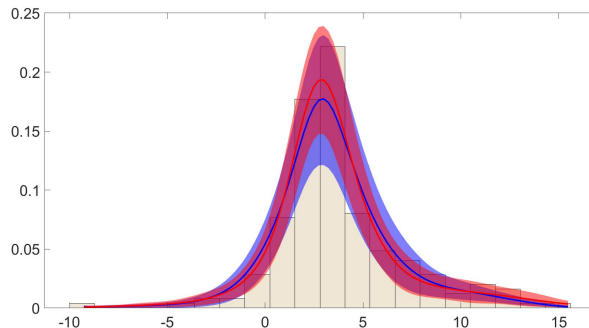
As a result

$$\int_{-\infty}^{\infty} f_x(\pi)_{t+h|t} dx = \sum_{i=2}^g \int_{\pi_{i-1}^*}^{\pi_i^*} f_x(\pi)_{t+h|t} dx = \sum_{i=2}^g \left[\sum_j^n \varphi_j + \int_{\pi_{i-1}^*}^{\pi_i^*} f_x(\pi)_{t+h} d\pi \right] = 1. \quad \blacksquare$$

E Additional Results

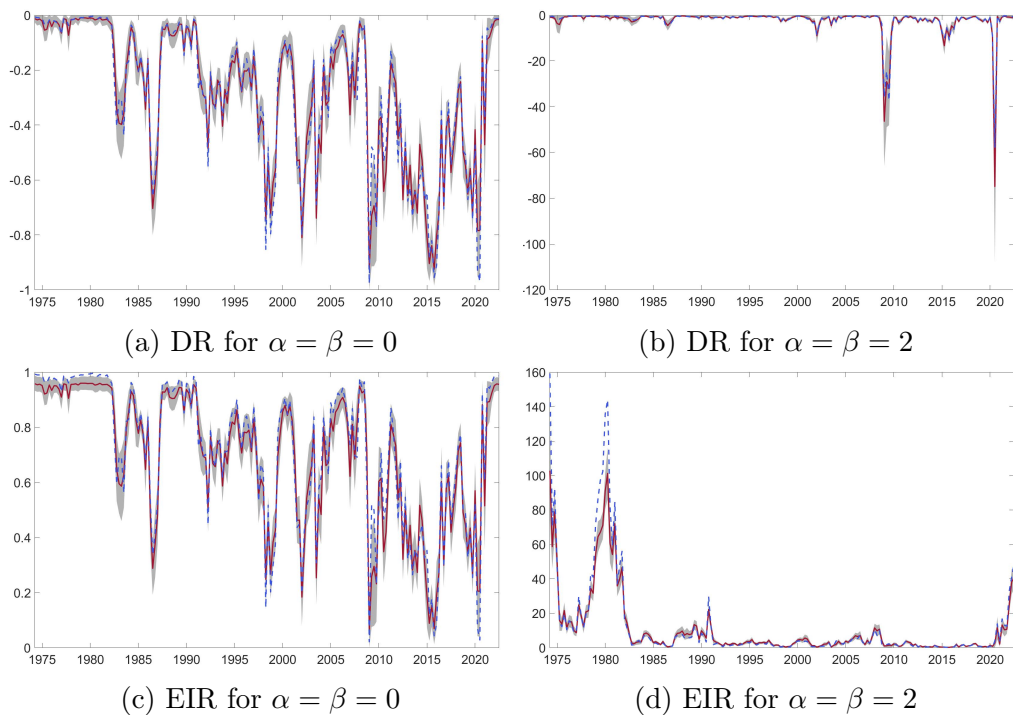
E.1 Additional Figures

Figure 7: Annualized Quarterly Inflation Density, MCMC and VB estimates



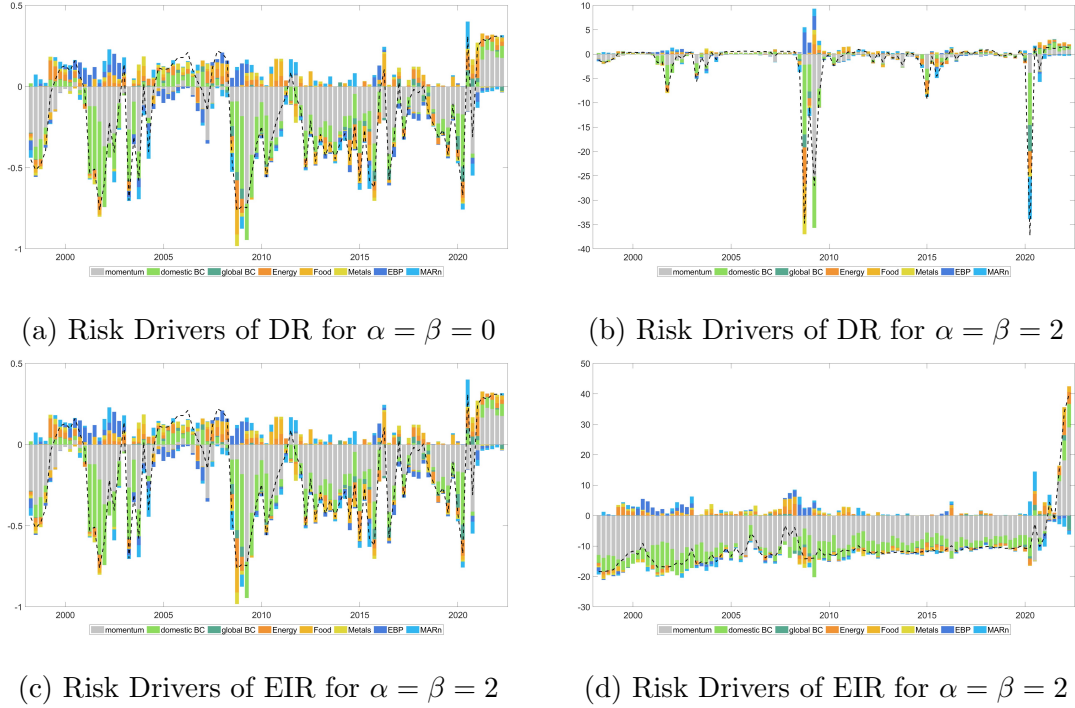
Notes: The histograms display the observed values for annualized quarterly inflation from 1974Q1 to 2022Q3 (beige). The blue (red) colored line and shaded area show the mean density estimate and 68% confidence bounds for MCMC (VB).

Figure 8: Historical Downside and Upside Risk



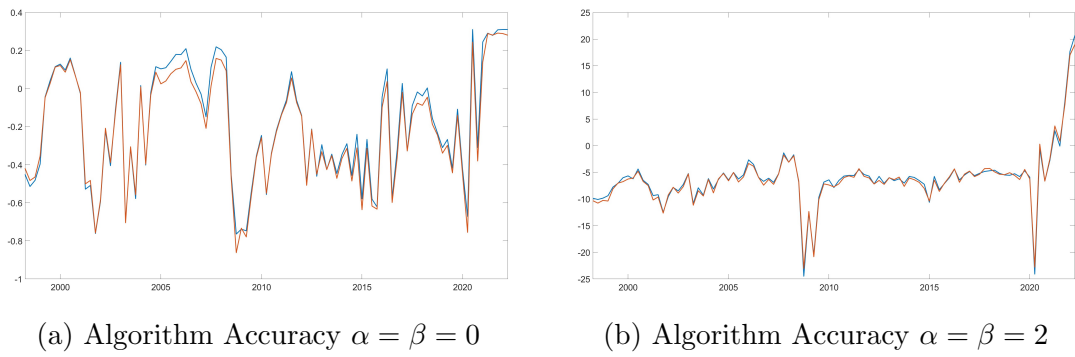
Notes: The solid red line indicates the MCMC estimate over the full sample. The shaded area is the corresponding 86% credible interval. The dashed blue lines show the VB estimate.

Figure 9: Drivers of the Balance of Risk



Notes: The coloured bars indicate the contribution of the corresponding variable to the balance of risk for the respective parameter setting. The dashed line indicates the observed value for the balance of risk minus the sample average.

Figure 10: Algorithm Accuracy



Notes: The blue line indicates the observed risk measure minus the sample average and the red line denotes the sum of the individual variable contributions.

E.2 Additional Tables

Table 4: Absolute RMSE

h	DR	AR	SV-AR	TVP-AR	TVPSV-AR	T-AR
1	2.031	2.322	2.196	3.005	2.793	2.291
2	2.224	2.698	2.382	5.173	2.951	2.586
3	2.392	2.805	2.487	6.174	2.667	2.669
4	2.501	2.738	2.474	7.67	2.553	2.624
8	2.461	2.917	2.421	4.408	2.849	2.597
12	2.911	3.343	2.835	5.655	3.472	2.770

The table shows the absolute RMSE for the density regression and the benchmark models for the forecast horizons $h = \{1, 2, 3, 4, 8, 12\}$.

Table 5: p-values for tests on PITs for all forecast horizons

	KS	AD	DH	Uniformity				Identical				Independent				Uniform				Identical				Independent								
				1 st		2 nd		1 st		2 nd		KS		AD		DH		1 st		2 nd		KS		AD		DH		1 st		2 nd		
				$H = 1$				$H = 2$				$H = 3$				$H = 4$				$H = 5$				$H = 6$				$H = 7$				
DR	0.871	0.735	0.214	0.979	0.740	1.000	0.597	0.489	0.364	0.158	0.180	0.966	0.240	0.112	0.280	0.365	0.475	0.037	0.835	0.135	0.100	0.521	0.407	0.288	0.000	0.000	0.102	0.043				
AR	0.007	0.002	0.000	0.322	0.000	0.607	0.097	0.015	0.004	0.000	0.001	0.000	0.884	0.532	0.003	0.002	0.000	0.001	0.002	0.487	0.297	0.000	0.000	0.000	0.000	0.000	0.000	0.000	0.000	0.000		
SV-AR	0.309	0.053	0.081	0.649	0.878	1.000	1.000	0.345	0.002	0.015	0.001	0.027	1.000	1.000	0.532	0.003	0.171	0.005	0.000	0.891	0.318	0.000	0.000	0.000	0.000	0.000	0.000	0.000	0.000	0.000		
TVP-AR	0.000	0.000	0.000	0.589	0.005	0.865	0.427	0.000	0.000	0.200	0.700	0.825	0.814	0.000	0.000	0.000	0.003	0.003	1.000	1.000	1.000	1.000	1.000	1.000	1.000	1.000	1.000	1.000	1.000			
TVP-AR	0.000	0.000	0.010	0.955	0.000	0.000	0.000	0.000	0.000	0.000	0.000	0.000	0.000	0.000	0.000	0.000	0.000	0.000	0.000	0.000	0.000	0.000	0.000	0.000	0.000	0.000	0.000	0.000	0.000	0.000		
T-AR	0.000	0.000	0.000	0.428	0.019	1.000	0.740	0.000	0.000	0.001	0.000	0.843	0.450	0.000	0.000	0.000	0.001	0.002	0.173	0.038	0.000	0.000	0.000	0.000	0.000	0.000	0.000	0.000	0.000			
QR	0.025	0.014	0.000	0.585	0.310	0.657	0.208	0.008	0.011	0.000	0.036	0.364	0.065	0.001	0.005	0.004	0.000	0.046	0.731	0.289	0.000	0.000	0.000	0.000	0.000	0.000	0.000	0.000	0.000			
DR	0.326	0.400	0.715	0.224	0.376	0.769	0.563	0.254	0.073	0.474	0.009	0.210	0.883	0.774	0.482	0.405	0.066	0.240	0.706	0.753	0.707	0.000	0.000	0.000	0.000	0.000	0.000	0.000	0.000	0.000		
AR	0.053	0.012	0.000	0.001	0.006	1.000	0.754	0.003	0.004	0.008	0.000	0.001	0.878	0.79	0.004	0.001	0.028	0.005	0.000	0.549	0.789	0.000	0.000	0.000	0.000	0.000	0.000	0.000	0.000	0.000		
SV-AR	0.382	0.000	0.105	0.005	0.002	1.000	0.748	0.236	0.001	0.050	0.008	0.002	1.000	0.628	0.278	0.003	0.564	0.001	0.000	0.848	0.293	0.000	0.000	0.000	0.000	0.000	0.000	0.000	0.000	0.000		
TVP-AR	0.000	0.000	0.005	0.044	0.274	0.150	0.000	0.000	0.002	0.189	0.342	0.308	0.000	0.000	0.000	0.000	0.000	0.235	0.371	0.522	0.672	0.000	0.000	0.000	0.000	0.000	0.000	0.000	0.000	0.000		
TVP-AR	0.000	0.000	0.056	0.000	0.931	0.000	0.000	0.000	0.002	0.003	0.899	0.000	0.000	0.000	0.000	0.000	0.000	0.017	0.005	0.907	0.000	0.000	0.000	0.000	0.000	0.000	0.000	0.000	0.000			
T-AR	0.000	0.000	0.000	0.004	0.009	0.429	0.133	0.000	0.000	0.001	0.036	0.350	0.104	0.000	0.000	0.000	0.000	0.007	0.028	0.481	0.372	0.000	0.000	0.000	0.000	0.000	0.000	0.000	0.000	0.000		
QR	0.000	0.002	0.000	0.053	0.234	0.550	0.137	0.000	0.000	0.159	0.199	0.820	0.400	0.000	0.000	0.000	0.000	0.000	0.227	0.630	0.854	0.598	0.000	0.000	0.000	0.000	0.000	0.000	0.000	0.000	0.000	
DR	0.335	0.065	0.681	0.004	0.768	0.825	0.841	0.173	0.054	0.892	0.045	0.612	0.670	0.801	0.213	0.391	0.470	0.009	0.189	0.180	0.686	0.000	0.000	0.000	0.000	0.000	0.000	0.000	0.000	0.000		
AR	0.001	0.000	0.028	0.002	0.003	0.246	0.564	0.000	0.000	0.015	0.003	0.000	0.201	0.428	0.000	0.000	0.000	0.000	0.000	0.104	0.264	0.000	0.000	0.000	0.000	0.000	0.000	0.000	0.000	0.000		
SV-AR	0.072	0.000	0.854	0.000	0.000	0.628	0.121	0.117	0.000	0.970	0.001	0.000	0.431	0.085	0.267	0.000	0.664	0.002	0.000	0.467	0.210	0.000	0.000	0.000	0.000	0.000	0.000	0.000	0.000	0.000		
TVP-AR	0.000	0.000	0.001	0.000	0.646	0.000	0.000	0.000	0.000	0.000	0.500	0.000	0.000	0.000	0.000	0.000	0.000	0.000	0.000	0.000	0.000	0.000	0.000	0.000	0.000	0.000	0.000	0.000	0.000	0.000		
T-AR	0.000	0.000	0.000	0.011	0.025	0.508	0.834	0.000	0.000	0.008	0.017	0.430	0.799	0.000	0.000	0.000	0.001	0.049	0.448	0.798	0.000	0.000	0.000	0.000	0.000	0.000	0.000	0.000	0.000			
QR	0.000	0.000	0.003	0.012	0.000	1.000	0.642	0.000	0.001	0.003	0.001	0.395	0.026	0.000	0.000	0.000	0.002	0.001	0.370	0.112	0.000	0.000	0.000	0.000	0.000	0.000	0.000	0.000	0.000			
DR	0.661	0.522	0.110	0.001	0.396	0.246	0.271	0.368	0.416	0.002	0.000	0.115	0.091	0.521	0.407	0.288	0.000	0.000	0.102	0.043	0.000	0.000	0.000	0.000	0.000	0.000	0.000	0.000	0.000			
AR	0.000	0.000	0.000	0.000	0.033	0.041	0.000	0.000	0.000	0.000	0.000	0.000	0.000	0.000	0.000	0.000	0.000	0.001	0.000	0.000	0.000	0.000	0.000	0.000	0.000	0.000	0.000	0.000	0.000	0.000		
SV-AR	0.214	0.000	0.839	0.003	0.586	0.185	0.260	0.000	0.655	0.000	0.000	0.071	0.058	0.099	0.000	0.263	0.002	0.000	0.000	0.000	0.000	0.000	0.000	0.000	0.000	0.000	0.000	0.000	0.000	0.000	0.000	0.000
TVP-AR	0.000	0.000	0.000	0.000	0.512	0.000	0.000	0.000	0.000	0.000	0.018	0.025	0.018	0.000	0.000	0.000	0.004	0.077	0.049	0.061	0.000	0.000	0.000	0.000	0.000	0.000	0.000	0.000	0.000	0.000		
T-AR	0.001	0.000	0.000	0.000	0.004	0.665	0.511	0.000	0.000	0.000	0.000	0.343	0.205	0.000	0.000	0.000	0.021	0.000	0.000	0.000	0.000	0.000	0.000	0.000	0.000	0.000	0.000	0.000	0.000	0.000	0.000	0.000
QR	0.000	0.000	0.000	0.000	0.000	0.161	0.054	0.000	0.000	0.000	0.000	0.043	0.021	0.000	0.000	0.000	0.000	0.000	0.000	0.000	0.014	0.016	0.000	0.000	0.000	0.000	0.000	0.000	0.000	0.000	0.000	

The table contains the p-values for several test statistics: KS=Kolmogorov-Smirnov, AD=Anderson-Darling, DH=Dornik-Hausen, Andrews, Liung-Box. For the Andrews and Liung-Box test, H^{st} and H^{nd} denote the results for the first and second moment, respectively. H indicates the forecast horizon. Bold values mark p-values greater than 5%.